Design Parameter Modeling of Solar Power Tower System Using Adaptive Neuro-Fuzzy Inference System Optimized with a Combination of Genetic Algorithm and Teaching Learning-Based Optimization Algorithm

A. Khosravi[1*], M. Malekan[2], J.J G. Pabon[3], X. Zhao[4], M.E.H. Assad[5]

[1] Department of Mechanical Engineering, School of Engineering, Aalto University, Finland
[2] Department of Engineering, Aarhus University, 8000 Aarhus C, Denmark
[3]Institute in Mechanical Engineering, Federal University of Itajubá (UNIFEI), Itajubá, Brazil
[4]School of Engineering, the University of Warwick, United Kingdom
[5]Department of Sustainable and Renewable Energy Engineering, University of Sharjah, UAE

* Corresponding author: Ali.khosravi@aalto.fi

Abstract

Determining the optimal sizing of a solar power tower system (SPTS) with a thermal energy storage system is subject to finding the optimum values of design parameters including the solar multiple (SM), design direct normal irradiance (DNI) and thermal storage hours. These design parameters are determined for each station separately and have remarkable effects on the thermo-economic performance of the system. This paper aims to demonstrate how artificial intelligence (AI) techniques may play an important role in addressing the above-mentioned need and help determine the optimum design parameters for different stations. For this purpose, we developed a thermo-economic model of a 100 MW SPTS with a molten salt storage system for five stations (two stations in India, and one each in Bangladesh, Pakistan, and Afghanistan). A method-based AI is utilized in this paper to ascertain the design parameters of the system. Additionally, a novel hybrid method based on adaptive neuro-fuzzy inference system optimized with a combination of genetic algorithm and teaching-learning-based optimization algorithm (ANFIS-GATLBO) is employed. The input parameters are latitude, longitude, design point DNI and SM, while the annual energy produced, levelized cost of energy and capacity factor are the target variables. The results of the study show that although the annual energy produced by SPTS rises by increasing the SM and decreasing design point DNI, optimum design parameters should be determined by the economic factors. In addition, it was found that the ANFIS-GATLBO method used in this study successfully predicted the targets with a correlation coefficient close to 1.

Keywords: Solar power tower system; Fuzzy system; Genetic algorithm; Teaching learning-based optimization algorithm; Artificial intelligence; Thermo-economic analysis

Nomenclature

A: area (m^2)
$C_{p,w}$: specific heat of water (J/kg K)
$\dot{C}$: thermal capacitance rate (W/K)
D_{tube}: the outer diameter of a single receiver tube [m]
F: view factor
h: convective heat transfer coefficient (W/m^2K)
h_s: main steam inlet enthalpy (KJ/kg)
h_c: additional condensate inlet enthalpy (KJ/kg)
h_{sat}: enthalpy of saturated water at P_{cond} (KJ/kg)
H_{helio}: height of the heliostat reflector (m)
I: beam normal solar radiation (W/m^2)
$\dot{m}$: mass flow rate (kg/s)
n_t: number of tubes in each panel
P''_{feild}: specific flux density on a receiver panel (W/m^2)
$\dot{Q}$: heat transfer rate (kW)
R_{cond}: conductive thermal resistance (K/W)
R_{conv}: convective thermal resistance (K/W)
T: temperature (℃)
W_{helio}: Work produced by the power cycle (W)

Greek Symbols
ρ_{field}: mirror reflectivity
η: efficiency
ΔP: pressure loss (Pa)
$\Delta T_{c,w}$: the temperature increase of the cooling water across the condenser (℃)
ΔAz: Azimuthal distance between heliostats [m]
ΔR: radial distance between heliostats [m]
$\eta_{thermal}$: receiver thermal efficiency

Subscripts/Superscripts
field: heliostat field
bn: beam normal
inc: incident
htf: heat transfer fluid
rec: receiver
helio: heliostat
min: minimum
max: maximum
cool: cooling water

1. Introduction

Fossil fuels such as crude oil, hard coal and natural gas used in combustion processes cause great damage to the environment, mainly due to greenhouse gas emissions [1,2]. These gas emissions lead to global warming. In addition, these sources of energy will soon be depleted, hence the need for sustainable alternatives. One of the most abundant available sources is solar energy [3,4]. It is one of the cleanest and most sustainable when compared to other renewable energy sources. However, the major challenge is how to successfully harness this energy and make it available for industrial application in the form of electricity [5]. One of the most efficient techniques is the use of solar towers. Solar power tower system (SPTS) use a heliostat which reflects solar heat onto a focus point (receiver point). Solar towers are the preferred technology in steam production and electricity generation [6].

The SPTS has the capability to meet high energy demands. Solar tower infrastructures are deemed considerably costly, while the output of most suitable energy production systems ranges from 30 to 400 MW [7,8]. In this energy production system, a heliostat field centralizes solar irradiance to a receiver located at the tower in order to heat up a working fluid. This system can be used in Rankine and Brayton cycles for steam generation or for preheating air before it enters the combustion chamber [9–11].

This paper proposes an intelligent method to simulate and appraise a 100 MW SPTS system by considering the fundamental design parameters. The optimal sizing of the SPTS with a thermal storage system is critical to achieving system reliability and reducing the cost of energy production. Design parameters are subject to the geographical features of the stations and are different for each specific region and the various solar resources. Hence, a network is constructed and trained to find the non-linear relationship between the latitude, longitude, design point direct normal irradiance (DNI), and solar multiple (SM) on the one hand and the annual energy produced by the system, levelized cost of energy (COE), and capacity factor. For this purpose, a novel intelligent method is devised based on adaptive neuro-fuzzy inference system (ANFIS) optimized through a combination of genetic (GA) and teaching-learning-based optimization (TLBO) algorithms. Following the common practice for dealing with prediction problems, ANN and fuzzy inference system (FIS) are employed. Combining these two methods results in ANFIS, which generally performs better than ANN and FIS. Furthermore, ANFIS parameters can be optimized with GA. In this study, to reach a better prediction performance, GA is combined with TLBO and employed to optimize the ANFIS.

2. Literature Review

Numerous research focuses on the process of optimising the heliostat field, specifically in thermal plants powered by SPTS. Wei et al. [7] proposed a new design approach of the heliostat field layout of the SPTS in order to save total design and optimization time. Whereas, Xu et al. [12] used a modular modelling method based on mathematical models in order to design a SPTS of 1 MW applying the first and second thermodynamic laws. They found that the highest exergy loss in the central receiver was cause by the heliostat mirror. Pitz-Paal et al. [13] presented an optimised technique for the layout of the heliostat field in order to maximize the annual solar-to-chemical energy conversion efficiency. This optimization algorithm utilized secondary optics, heliostat characteristics, and chemical receiver–reactor characteristics.

In another study, Ozturk and Dincer [14] presented an analysis of an SPTS integrated into a coal gasification system using thermodynamic-based approaches. Avila-Marin et al. [15] investigated a parametric analysis of a medium to large (290–500 MW) central receiver SPTS using four steps: size and location analysis, technology analysis, storage analysis, and component cost analysis. A method of increasing steam parameters developed by Singer et al. [16] led to raising thermal efficiency and the total net efficiency of the entire SPTS. In addition, Benammar et al. [8] presented a numerical model to analyse and simulate the performance of SPTSs. Moreover, an efficient computational design method of a heliostat field for the SPTS was offered by Besarati and Goswami [17]. Their model led to an optimization of around 50 MW in terms of heliostat field design. In an investigative study, Al-Sulaiman and Atif [18] conducted an analysis and consequence comparison of the performance of carbon dioxide Brayton cycles used as assistance for the SPTs. Their results show thermal efficiencies of 42% and 52% for Brayton cycle and for the integrated overall cycle, respectively. Collado et al. [19] proposed a two-steps optimization technique for collector field of an SPTS by breaking the optimization process down into two sequential steps: a primary/energy optimization (independent of the cost models) and a main/economic optimization. Their optimum designs mainly depended on electricity tariff, receiver cost, and the supposed maximum surface temperature of the receiver. Moreover, an analysis of an SPT for high- temperature electrolyzer used for hydrogen production was presented by AlZahrani and Dincer [20]. They reported a rate of efficiency of the overall solar-hydrogen conversion system of around 12.7% and 39.5% for charging and discharging thermal energy storage system cases, respectively. An energetic and exergetic analysis was performed by Atif and Al-Sulaiman [21] of a carbon dioxide recompression cycles driven by an SPTS for six different locations in Saudi Arabia. Their results showed that the maximum and minimum annual exergy destructions are around 200 MW for Dhahran and 174 MW for Madinah. Chen et al. [22] presented a thermo-economic model for a 50 MW SPTS depending on the steam Rankine cycle with molten salt (MS) storage. The aim of their work was to explore the optimal combinations of different parameters at four sites in China. A mathematical model was built by Zhang et al. [23] in order to investigate the characteristics of the steam generation system in an SPTS after static validation. More recently, Kalathakis et al. [24] proposed a simulation environment allowing both steady-state and transient modelling to perform everyday operation and maintenance management for an SPTS.

While there have been many studies conducted on direct steam generation in parabolic trough solar power plants (see e.g. [25–29]), the SPTS with energy storage system has received less attention. As a matter of fact, the use of SPTS in energy generation is still in its early stages, with very few industrial applications [30,31]. Currently, there are only four plants using this technology in central receiver plants in the world [32]: PS10 and PS20 (both located in Spain), Khi Solar One (located in South Africa), and Ivanpah Solar Project (located in United States). Economic and exergetic analyses by González-Gómez et al. [33] and Gómez-Hernández et al. [34] have shown steam generator relevance to the whole SPTS performance. Gómez-Hernández et al. [35] proposed a new steam generator design with dual-pressure level evaporation working with a higher inlet pressure up to 165 bar, aiming to improve the power block efficiency. This new approach was shown to result in an increase in power block efficiency from 44.14% to 44.64%. Furthermore, Li et al. [36] proposed a new approach to solving low storage capacity of the accumulators by using two-stage accumulators and steam-organic Rankine cycles. They [37] developed a coupled 3D receiver cavity heat transfer with a 1D two-phase flow model for a solar receiver with indirectly irradiated absorber tubes for the direct steam generation. Their results showed that parameters such as tube types, in terms of multiple and helical tubes, fluid inlet position, surface emissivity, flow rates, target

operation temperature, and incoming solar power have significant impact on the performance of the direct steam generation system. More recently, a direct steam cycle assisted SPTS, in which weather conditions were taken into consideration, was designed for Iskenderun-Turkey region by Yagli et al. [38]. Table 1 below presents a summary of different research studies that dealt with modelling of the SPTS system.

Table 1. Studies on modelling of solar power tower system.

Author	Capacity (MW)	Type analysis*	Transient state model	Storage system	Cycle generation
Xu et al. [12]	1.0	En	Yes	Yes	Rankine
Xu et al. [39]	1.8	En-Ex	No	No	Rankine
Ozturk and Dincer [14]	300	En-Ex	No	Yes	Rankine/Brayton
Avila-Marin et al. [15]	100-500	En-Ec	No	Yes	Rankine
Benammar et al. [8]	0.1	En	No	No	Rankine
Al-Sulaiman and Atif [18]	0.1	En	No	No	Brayton
AlZahrani and Dincer [20]	0.5	En-Ex	No	Yes	Brayton
Atif and Al-Sulaiman [21]	40	En-Ex	No	No	Brayton
Chen et al. [22]	50	En-Ec	No	Yes	Rankine
Zhang et al. [23]	35	En	Yes	No	Rankine
Kalathakis et al. [24]	45	En	No	No	Brayton
Gómez-Hernández et al. [34]	110	En-Ex-Ec	No	Yes	Rankine

*En=energy, Ex=exergy, Ec=economic

Non-linear relationships between the various design parameters of an SPTS make it difficult to obtain a reliable mathematical function to predict and optimize these systems using conventional methods. Artificial neural networks (ANNs) are efficient tools that predict patterns too complex for humans to find and taught machines to recognize [40]. ANN-based methods have been successfully developed in the solar energy research to predict, optimize design, and evaluate different solar radiation parameters [41–46]. Alnagi et al. [47] proposed a hybrid method based on ANN incorporated with particle swarm optimization for predicting the energy performance of a building integrated photovoltaic/thermal system. Mittal et al. [48] implemented an ANN to predict the performance of a photovoltaic system as a function of solar irradiance and ambient temperature. Yousif et al. [49] simulated a photovoltaic/thermal solar energy system using ANN. To the best of our knowledge, there has not been any studies that deal with modelling of SPTS using ANN, except the work of López et al. [50], in which they developed an ANN approach to analyse water vapour effect on the atmospheric transmission loss of solar radiation between heliostats and the receiver of an SPTS. The model was able to deliver the direct normal irradiance for a variety range of input data, with a root mean square differences of 0.8%.

3. Solar Power Tower System (SPTS)

The availability of solar radiation varies according to the location of the SPTS plant. Figure 1 below represents the solar map for stations under study where the value of global horizontal irradiance is cited (for long-term average data, 1999-2015). These stations are located in different regions and have been intentionally selected for this reason. Table 2 below shows the exact location of each station (New Delhi, India; Thanjavur, India; Dhaka, Bangladesh; Kabul, Afghanistan; and Islamabad, Pakistan). It is apparent that these stations have remarkable potential for solar radiation with global horizontal irradiance higher than 5 ($kWh/m^2.day$).

Table 2. The considered stations [51].

	Station	Latitude	Longitude	Station ID
1	New Delhi, India	28.65	77.25	33896

2	Thanjavur, India	10.75	79.15	39987
3	Dhaka, Bangladesh	23.85	90.45	77408
4	Kabul, Afghanistan	34.55	69.25	7555
5	Islamabad, Pakistan	33.65	73.05	20086

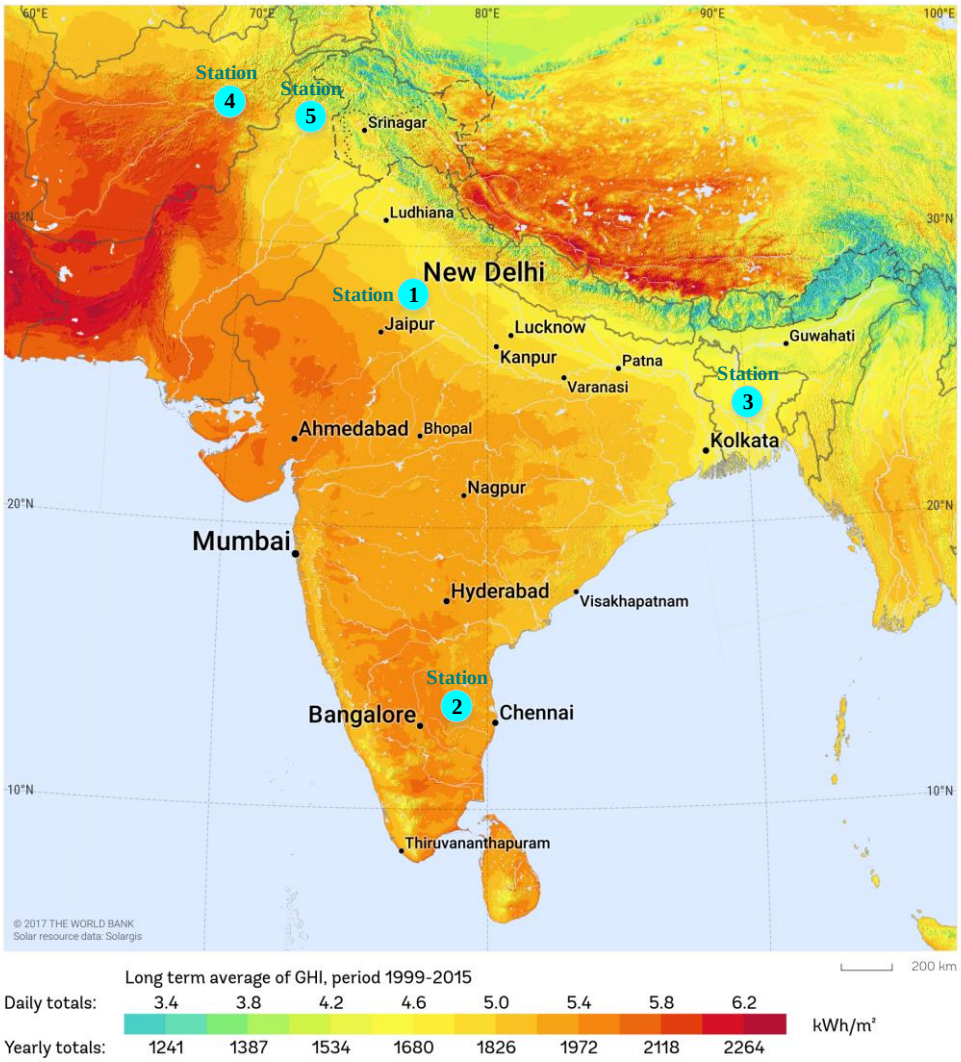

Fig. 1. Solar map of the global horizontal irradiance for the studied stations [52].

SPT is a type of concentrating solar system that generates electrical power by reflecting the high flux solar radiation onto a relatively small receiver. The receiver can be equated to the boiler in a traditional electricity generation cycle such as Rankine or Brayton. In addition, a heat transfer fluid is used to absorb heat directly or by contact with the receiver surface. In some cases, the solar tower system is employed to facilitate a chemical process like electrolysis. In contrast to other prominent alternative renewable energy technologies, such as wind and photovoltaic, the thermal energy produced by the solar tower system can be stored for later use. Fig. 2 demonstrates a solar power tower system incorporated with MS energy storage system. It is composed of five segments: power cycle, balance of plant, thermal storage, tower and receiver, and heliostat field.

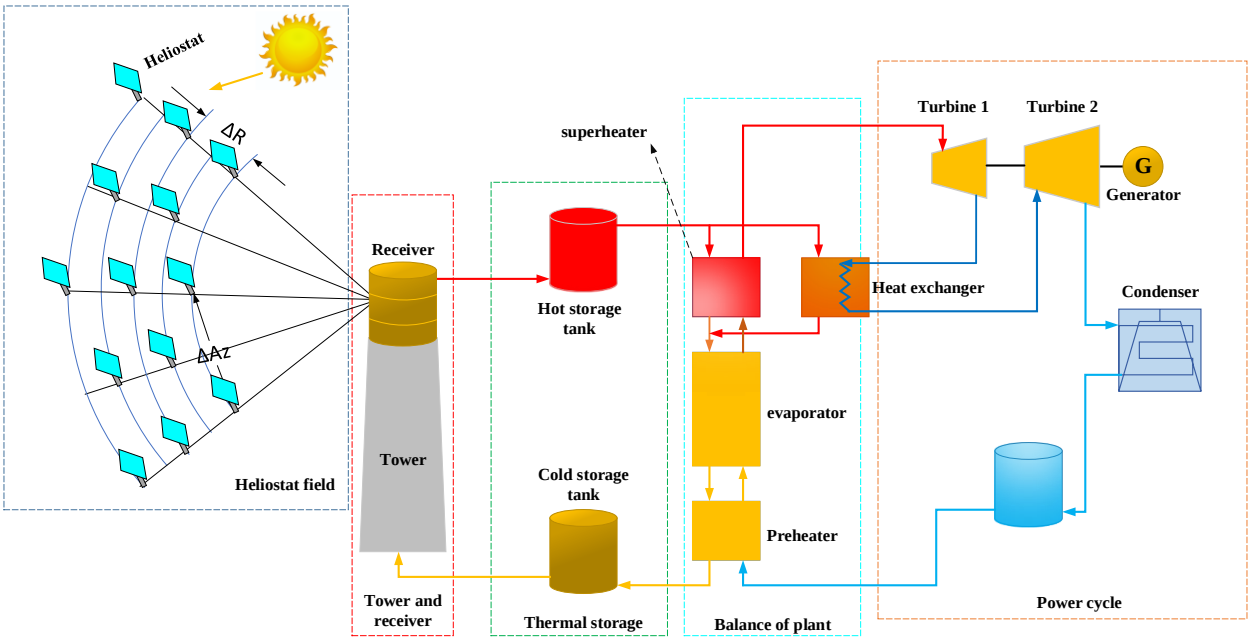

Fig. 2. A schematic of solar power tower system with MS storage system [51].

3.1. Heliostat Field

The array of planer mirrors is adjusted to achieve highly concentrated solar radiation on the central receiver. The total power incident on the receiver surface ($\dot{Q}_{inc}$) is calculated by [22]:

$$\dot{Q}_{inc} = A_{field}.\eta_{field}.DNI \tag{1}$$

where A_{field}, η_{field}, and DNI are the surface field area, total heliostat field efficiency and direct normal irradiance, respectively. In this instance, an optimization algorithm,DELSOL3 [51], is employed to determine the optimum values of A_{field} and η_{field} for different stations, and different values of design point DNI and SM. One distinct advantage of solar power tower system, compared to the other solar systems such as linear Fresnel and parabolic through, is that the central receiver works at a higher thermal efficiency, which leads to the absorption of more solar energy by the system. This is due to the high incident of flux concentration on the central receiver, which is achieved by heliostats. In order to attain maximum performance, the average distance between the heliostats and tower, installation, accurate construction and control of the heliostats must be taken into account. To design a heliostat field, the optimizing code (DELSOL3) [53] is employed, which is established based on radial and azimuthal spacing correlations:

$$\Delta R = (1.1442 \cdot cot\theta_L - 1.0935 + 3.0684\theta_L^2)H_{helio} \tag{2}$$

$$\Delta Az = (1.791 + 0.6396 \cdot \theta_L) \cdot W_{helio} + \frac{0.02873}{\theta_L - 0.04902} \tag{3}$$

where $\theta_L = (\pi/2) - \theta_t$, θ_t is the angle between a vector from the heliostat to the tower and vertical, H_{helio} is the heliostat height, and W_{helio} is the heliostat width.

3.2. Central Receiver

A simple model for tower receiver was proposed by Jones of Sandia National Labs [51] in which the thermal efficiency of the receiver is considered as an input variable. As can be seen in Eq. (2), this model supplies the required mass flow rate ($\dot{m}_{htf,demand}$) to reach a temperature set-point as an output [53].

$$\dot{m}_{htf,demand} = \frac{\dot{Q}_{inc}.\eta_{rec}}{\left(c_{htf}.\left(T_{htf,hot} - T_{htf,cold}\right)\right)} \tag{4}$$

where η_{rec}, c_{htf}, $T_{htf,hot}$, and $T_{htf,cold}$ are tower thermal efficiency, heat transfer fluid (HTF) specific heat, HTF outlet temperature set-point, and HTF inlet temperature, respectively.

Crespo [53] developed a new method that takes the variable tower efficiency into account by scaling it with the ratio of the incident power (C_{oc}) to the receiver design thermal power. This, along with the ratio of part-load efficiency to the design efficiency (C_{eff}), are correlated by employing a hyperbolic fit (here, *a* and *b* are additional parameters that are calculated to aid the process).

$$C_{oc} = \frac{\dot{Q}_{partload}}{\dot{Q}_{design}} \tag{5}$$

$$C_{eff} = \frac{\eta_{partload}}{\eta_{design}} \tag{6}$$

$$a = \frac{(1 - C_{oc})\eta_{partload}}{C_{eff} - C_{oc}} \tag{7}$$

$$b = \left(\frac{a}{\eta_{design}}\right) - 1 \tag{8}$$

After achieving the coefficients, the ratio (W_{pl}) of the incident power to the design incident thermal power is derived and the total efficiency is calculated.

$$W_{pl} = \left(\frac{\dot{Q}_{inc}}{3600}\right)\frac{1}{\dot{Q}_{design}} \tag{9}$$

$$\eta_{tot} = \frac{a.W_{pl}}{b + W_{pl}} \tag{10}$$

Moreover, the capacity factor is defined as the ratio of the system predicted electrical output in the first operational year to the nameplate output. This is equivalent to the quantity of energy the system would generate if it operated at its nameplate capacity for the whole year.

Figure 3 below illustrates the thermodynamic model of receiver. The receiver model is a basic building block with a length of Δx. This element is modelled by considering the multiple heat transfer mechanisms including incident radiation ($\dot{q}_{inc}$), external convection ($\dot{q}_{conv}$), radiation exchange to environment ($\dot{q}_{rad}$) and radiation reflected from the tube surface ($\dot{q}_{ref}$).

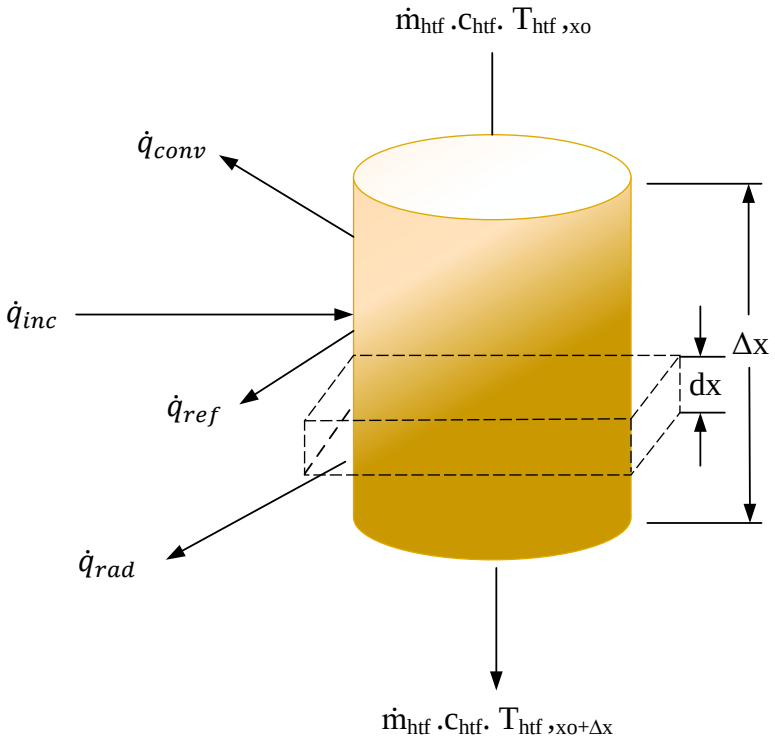

Fig. 3. Energy balance for a receiver tube element.

The overall steady-state energy balance for each differential element *dx* is determined by [22]:

$$\dot{q}_{fluid} = \dot{q}_{inc} - (\dot{q}_{ref} + \dot{q}_{rad} + \dot{q}_{conv}) \tag{11}$$

The terms used in Eq. (11) can be presented as integrals over the length of the element (Δx) with respect to the axial position (x). The integral form of the incident irradiative flux is written as [53]:

$$\dot{q}_{inc}(x) = D_{tube} n_t . \int_{x_0}^{x_0+\Delta x} P^{"}_{feild}(x) dx \tag{12}$$

$$\dot{q}_{inc,x} = P^{"}_{feild} . \Delta x . D_{tube} . n_t \tag{13}$$

in which $P^{"}_{feild}$ is the flux distribution and n_t is number of tubes in each panel. The reflected energy from the tower is presented by [53]:

$$\dot{q}_{ref}(x) = (1-\alpha) . D_{tube} . n_t . \int_{x_0}^{x_0+\Delta x} P^{"}_{feild}(x) dx \tag{14}$$

$$\dot{q}_{ref,x} = (1-\alpha) . D_{tube} . n_t . P^{"}_{feild} . \Delta x \tag{15}$$

where α is hemispherical absorptivity for the tower surface (since the tower surface is opaque, the reflectivity is $(1-\alpha)$).

The rate of heat transfer radiation is [53]:

$$\dot{q}_{rad}(x) = \sigma \varepsilon \pi . \frac{D_{tube}}{2} F_{t,s} . n_t . \int_{x_0}^{x_0+\Delta x} (T_s^4(x) - T_{amb}^4) dx \tag{16}$$

$$\dot{q}_{rad,x} = \sigma\varepsilon\pi.\frac{D_{tube}}{2}F_{t,s}.n_t.\left(T_{s,x}^4 - T_{amb}^4\right)\Delta x \quad (17)$$

in which ε is emissivity considering as 0.88 and $F_{t,s}$ is the view factor equalling to 0.6366. The convective loss is defined as a portion of temperature difference between external surface of the receiver tube and free stream air temperature.

$$\dot{q}_{conv}(x) = h_m.D_{tube}.n_t.\int_{x_0}^{x_0+\Delta x}(T_s(x) - T_{amb})dx \quad (18)$$

$$\dot{q}_{conv,x} = h_m.D_{tube}.n_t.\Delta x.\left(T_{s,x} - T_{amb}\right) \quad (19)$$

Finally, the thermal energy adding to the working fluid ($\dot{q}_{fluid}$) is defined by [53]:

$$\int_{x_0}^{x_0+\Delta x} dT_{hft} = \int_{x_0}^{x_0+\Delta x}\frac{\dot{q}_{fluid}(x)}{\dot{m}_{hft}.c_{hft}(x)}dx \quad (20)$$

$$T_{htf,x_0+\Delta x} - T_{hft,x_0} = \frac{\dot{q}_{fluid,x}.\Delta x}{\dot{m}_{hft}.c_{hft,x}} \quad (21)$$

The conduction and convective resistances between the inner tube wall and the working fluid are presented by Eqs. (22) and (23), respectively.

$$R_{cond} = \frac{ln\left(\frac{D_{tube}/2}{D_{inner}/2}\right)}{(\pi.2.\Delta x.k_{tube}.n_t)} \quad (22)$$

$$R_{conv} = \frac{1}{\left(h_{inner}.\Delta x.D_{inner}.{}^{\pi}/_{2}.n_t\right)} \quad (23)$$

The difference in temperature for the heat transfer is derived by [53]:

$$T_{s,x} - T_{htf,ave,x} = \dot{m}_{hft}.c_{hft,x}.\left(T_{hft,x_0+\Delta x} - T_{hft,x_0}\right)(R_{cond} + R_{conv}) \quad (24)$$

3.3. Thermal Energy Storage and Rankine Cycle System

The SPTS is considered with molten salt (MS) for thermal storage system (TES). Molten salt is a type of thermal energy storage system, which has been considered as storage system here. Due to the various operation modes present, two thermal storage tanks are considered with which the mass and energy balance are controlled. The mass balance of each one is determined by the following equation [54]:

$$m_{MS,new} = m_{MS,ini} + \left(m'_{MS,in} + m'_{MS,out}\right).t_{int} \quad (25)$$

Here, $m_{MS,new}$, $m_{MS,ini}$, $m'_{MS,in}$, $m'_{MS,out}$ and t_{int} are the mass in each tank after time interval, mass before time interval, mass flow rate of MS in and out of each tank, and interval of time, respectively. For each time interval, the energy balance relation is [54]:

$$\frac{dE_t}{dt} = h_{in}.\frac{\delta m_{MS,in}}{dt} - h_{out}.\frac{\delta m_{MS,out}}{dt} - \frac{\delta Q_{loss,tan\,k}}{dt} \quad (26)$$

in which E_t, h_{in}, h_{out} are energy increment in tanks, specific enthalpy of MS entering and leaving hot tank respectively. Moreover, $m_{MS,in}$ and $m_{MS,out}$ are mass of MS flow into and out of the tanks within the infinitesimal time; $Q_{loss,tan\,k}$ is the heat loss of MS in the tanks.

As for the generation cycle, Table 3 epitomizes the main formulation of the Rankine cycle components including heat exchangers, evaporator, turbine, and condenser.

Table 3. Summarized formulation of the Rankine cycle [53].

Economizer, superheater for water/steam heated by one phase fluid	
$\eta_{ECO} = \frac{1 - exp\left(-\frac{UA}{\dot{C}_{min}}.\left(1 - \frac{\dot{C}_{min}}{\dot{C}_{max}}\right)\right)}{1 - \frac{\dot{C}_{min}}{\dot{C}_{max}}.exp\left(-\frac{UA}{\dot{C}_{min}}.\left(1 - \frac{\dot{C}_{min}}{\dot{C}_{max}}\right)\right)}$	(27)
$UA = UA_{ref}.\left(\frac{\dot{m}_{cold}}{\dot{m}_{cold,ref}}\right)^{UA\_exp}$	(28)
$\Delta P = \Delta P_{ref}.\left(\frac{\dot{m}_{cold}}{\dot{m}_{cold,ref}}\right)^{\Delta P\_exp}$	(29)
Evaporator	
$\eta_{Evaporator} = 1 - exp\left(\frac{-UA}{\dot{m}_{hot}.c_{p,hot}}\right)$	(30)
$\dot{Q}_{trans} = \eta_{Evaporator}.c_{p,hot}.\dot{m}_{hot}.\left(T_{hot,in} - T_{saturated}\right)$	(31)
Turbine	
$P_{in} = \sqrt{\left(\frac{\dot{m}_{in}}{\dot{m}_{ref}}\right)^2\left(P_{in,ref}^2 - P_{out,ref}^2\right) + P_{out}^2}$	(32)
$\eta_{in,turbine} = \eta_{in,ref}.\left(1 + \alpha.\dot{m}_{ratio} + \beta.\dot{m}_{ratio}^2 + \gamma.\dot{m}_{ratio}^3\right)$	(33)
$\dot{m}_{ratio} = \frac{\dot{m}_{in}}{\dot{m}_{ref}} - 1$	(34)
Condenser	
$\dot{Q}_{cond} = h_s.\dot{m}_s + h_c.\dot{m}_c - (\dot{m}_s + \dot{m}_c).h_{sat}$	(35)
$\dot{m}_{cool} = \frac{\dot{Q}_{cond}}{C_{p,w}.\Delta T_{c,w}}$	(36)

3.4. Levelized Cost of Energy (COE)

One of the most attractive economic criteria is levelized cost of energy (COE) that indicates the total project lifecycle cost. The following equation is applied to compute the levelized COE [22]:

$$LCOE = \frac{C_{invest}\left(f_{annuity} + f_{ins,ann}\right) + C_{o\&m,ann}}{E} \quad (37)$$

in which C_{invest}, $C_{o\&m,ann}$, $f_{ins,ann}$ are capital cost of the system comprising all subsystem costs; the costs of operation and maintenance; and the annual insurance rate, respectively. In addition, $f_{annuity}$ is calculated by [22]:

$$f_{annuity} = \frac{(1+i)^n.i}{(1+i)^n - 1} \quad (38)$$

in which i is discount rate, and n is the lifetime.

3.5. Simulation Scenarios

Table 4 represents the technical specifications of the simulated SPTS. The predicted scenarios for the SPTS are presented in Table 5. The system was investigated by different values of design point DNI and SM in various stations.

Table 4. Technical properties of the designed SPTS.

Parameter	Value	Parameter	Value
Design turbine gross output	100 MWe	Condenser type	Air-cooled
Estimated gross to net conversion factor	0.9	$T_{ambient}$ at design	42 ℃
HTF hot temperature	574 ℃	Tank height	12 m
HTF cold temperature	290 ℃	System costs	
Heliostat width	12.2 m	Site improvement costs	16 $/m^2
Heliostat height	12.2 m	Heliostat field cost	140 $/m^2
Heliostat deploy angle	8 deg	TES cost	22 $/kWht
Tube outer diameter	40 mm	Balance of plant cost	290 $/kWe
Tube wall thickness	1.25 mm	Power cycle cost	1040 $/kWe
Boiler operating pressure	100 bar	Annual interest rate	7%

Table 5. The considered scenarios for each station.

Scenario	Design point DNI (W/m2)	SM	Scenario	Design point DNI (W/m2)	SM
1	1100	2.4	15	850	1.5
2	950	2.4	16	750	1.5
3	850	2.4	17	650	1.5
4	750	2.4	18	550	1.5
5	650	2.4	19	1100	2.8
6	550	2.4	20	950	2.8
7	1100	2	21	850	2.8
8	950	2	22	750	2.8
9	850	2	23	650	2.8
10	750	2	24	550	2.8
11	650	2	25	500	3
12	550	2	26	500	3.5
13	1100	1.5	27	500	4
14	950	1.5			

4. Intelligent Methods

As described above, simulating a SPTS is a complicated task that needs the implementation of sophisticated mathematical modelling. In this paper, an intelligent model is proposed to simulate a SPTS equipped with MS storage system, as can be seen in Fig. 4. The SPTS was investigated for five stations by considering 27 scenarios each. The obtained data was used to train a network. This network was constructed by latitude (°), longitude (°), design point DNI (W/m^2) (enhancing this parameter shows that fewer heliostats are required to obtain the reference condition power, while reducing this parameter has the inverse effect) and SM (solar multiple ascertains the receiver's nominal thermal power and is defined as the ratio of receiver to the cycle thermal powers) as input parameters. Three main parameters of the SPTS, including the annual energy produced by the system, levelized COE ($/kWh) and capacity factor (%), are selected as the targets. Data is obtained from energy modelling of the system in System Advisor Model (SAM). As can be seen in Fig. 4a, the data is divided into two distinct sets (70% for training the network and 30% for testing the model).

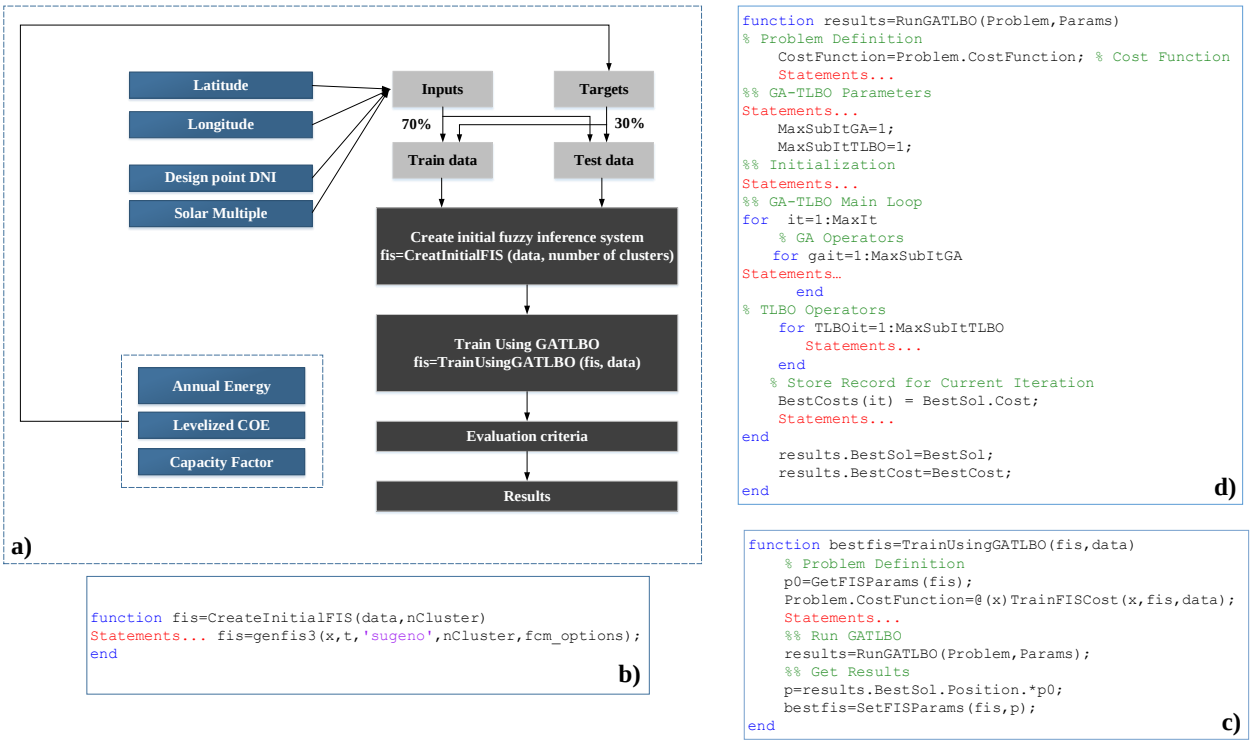

Fig. 4. The proposed structure for modelling the SPTS with intelligent method.

The intelligent method is an adaptive neuro-fuzzy inference system (ANFIS), a type of machine learning algorithms, which is generated based on Takaki-Sugeno's fuzzy logic system. This method combines fuzzy logic and artificial neural network (ANN) principles to utilize the benefits of both in one structure. ANFIS interface system is based on a set of fuzzy IF-THEN rules, which have learning capabilities to estimate nonlinear functions. Commonly radial basis function neural network is integrated into fuzzy logic to create an ANFIS model. The structure of ANFIS is constructed based on five layers. Layer 1 is called the fuzzification layer. The output of each node in the fuzzification layer is calculated by the **Error! Reference source not found.**9) and **Error! Reference source not found.**0) [55].

$$O_1^i = \mu_{A_i}(x), \qquad for\ i = 1,2 \tag{39}$$

$$O_1^i = \mu_{B_{i-2}}(y), \qquad for\ i = 3,4 \tag{40}$$

where x and y are the input nodes, A and B are the linguistic labels, μ_x and μ_y are the membership functions with a Gaussian shape in the range of 0 and 1. The membership function is demonstrated in **Error! Reference source not found.**) and **Error! Reference source not found.**):

$$\mu_{(x)} = \frac{1}{1+\left(\frac{x-c_i}{a_i}\right)^{2b_i}}, \tag{41}$$

$$\mu_{(x)} = \exp\left\{-\left(\frac{x-c_i}{a_i}\right)^2\right\}, \tag{42}$$

in which x is the input and $\{a_i, b_i, c_i\}$ are premise parameters (parameter set). The shape of the membership function varies according to the values of these parameters.

Layer 2 is the rule layer. Nodes in this layer are fixed and calculate the firing strength of a rule (w_i).

$$O_2^i = w_i = \mu_{A_i}(x)\,\mu_{B_i}(y), \qquad for\ i = 1,2 \tag{43}$$

In Layer 3, which is referred to as the normalization layer, the fixed node function normalizes the firing strength by calculating the ratio of the ith node firing strength to the sum of all:

$$O_3^i = \bar{w}_i = \frac{w_i}{w_1 + w_2}, \qquad for\ i = 1,2 \tag{44}$$

The next layer is the defuzzification layer; every node in layer 4 is an adaptive node with the node function of:

$$O_4^i = \bar{w}_i f_i = \bar{w}_i (p_i x + q_i y + r_i), \qquad for\ i = 1,2 \tag{45}$$

where $\bar{w}_i$ is the output of Layer 3, $\{p_i . q_i . r_i\}$ are the resultant parameters, and f_1 and f_2 are the fuzzy if-then rules.

Layer 5 is the output layer. The output node in layer five aggregates all received signals from the former layer. The relation for the output node is presented in **Error! Reference source not found.**).

$$O_5^i = \sum \bar{w}_i f_i = \frac{\sum_i w_i f_i}{\sum_i w_i} = overall\ output, \qquad for\ i = 1,2 \tag{46}$$

The final output of the ANFIS method can be represented as a linear combination of the resulting parameters. The final output in **Error! Reference source not found.** can be explained by:

$$\begin{aligned} f_{out} &= \bar{w}_1 f_1 + \bar{w}_2 f_2 = \frac{w_1}{w_1 + w_2} f_1 + \frac{w_2}{w_1 + w_2} f_2 \\ &= (\bar{w}_1 x) p_1 + (\bar{w}_1 y) q_1 + (\bar{w}_1) r_1 + (\bar{w}_2 x) p_2 + (\bar{w}_2 y) q_2 + (\bar{w}_2) r_2 \end{aligned} \tag{47}$$

As has rightly been pointed out in previous research, ANFIS has two main parameters: premise and consequent. In this case, the optimum values of these parameters are determined by a combination of genetic and teaching-learning-based optimization algorithms (GA and TLBO). GA is a popular method developed based on natural selection. TLBO is a type of evolutionary optimization algorithm that was developed by Rao et al. [56]. This method was derived from observations of the influence of a teacher on his/her learners. It is a population-based algorithm, which employs a population of solutions to proceed to the global solution. In this instance, a population is defined as a class or a group of learners. Figure 5 represents a flowchart of TLBO for an optimization process [56]. As can be seen, this process is divided into two main steps: “Teacher Phase” and “Student Phase”. The first section is implemented based on learning from the teacher and the second section is developed based on learning through interaction among learners. More details regarding TLBO can be found in [56,57].

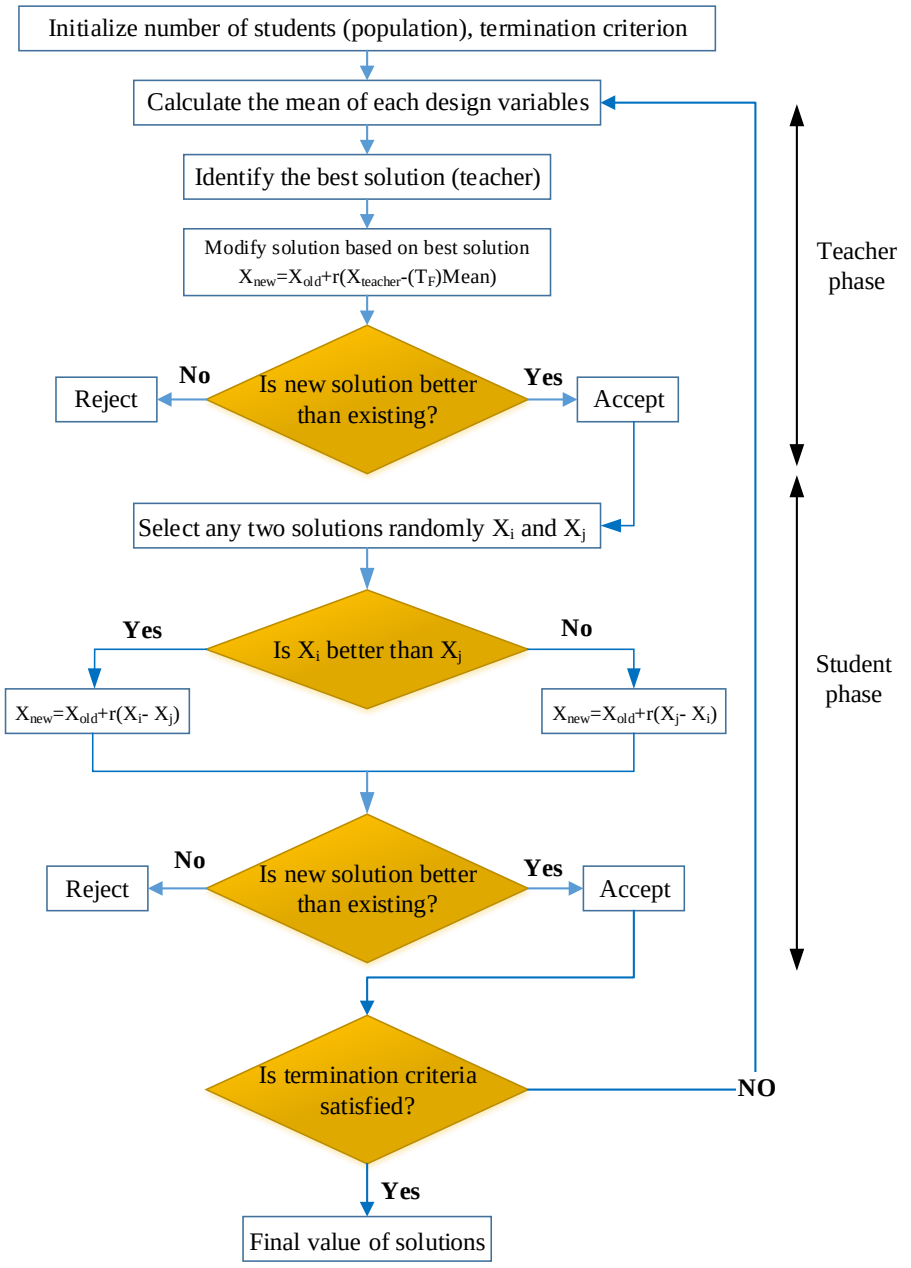

Fig. 5. A schematic of TLBO algorithm [56].

Figure 4a represents a summary of the main structure of the ANFIS-GATLBO to model the SPTS. Step 1 is establishing the input parameters and target. Step 2 is to divide the train and test samples. Step 3 is generating an initial fuzzy inference system (FIS) by employing a function (CreateInitialFIS) depicted in Fig. 4b. For this target, *genfis3* in Matlab software is applied, which uses fuzzy c-means (FCM) clustering by exploiting a set of rules modelling data behaviour. This function receives input data and number of clusters as input arguments. In step 4, the developed model is trained through a combination of GA and TLBO algorithm. The function of TrainUsingGATLBO is presented in Fig. 4c. The problem is implemented as determining the optimum values for basic FIS parameters. The basic values of FIS parameters are presented as $P_1^0, P_2^0, \dots, P_n^0$ and the optimum values of these parameters are assumed $P_1^*, P_2^*, \dots, P_n^*$. The optimization problem is defined as Eq. (48). The best value of x is determined by using GATLBO algorithm as described in Fig. 4d.

$$P_i^* = x_i \, P_i^0 \tag{48}$$

5. Result and Discussion

In this research project a thermo-economic analysis for a 100 MW SPTS equipped with molten salt (MS) storage systems in five different stations has been developed using System Advisor Model (SAM) [51]. The main design parameters of these stations (including design point DNI, solar multiple, and solar field hours of storage) have been determined to obtain the minimum levelized COE. For each station, 27 scenarios were defined in which the number of heliostats, tower height, receiver diameter, annual energy, levelized COE, capacity factor and net capital cost have been calculated. For designing a SPTS, the number of heliostats, tower and receiver heights, and receiver diameter are determined by employing an optimization process. The local derivate free (DFO) algorithm used in SAM is employed to optimize the power plant configuration. Based on data collected for each station, we proposed an intelligent method to model the behaviour of SPTS equipped with a MS storage system. The proposed intelligent model was ANFIS optimized with a combination of genetic and teaching-learning-based optimization algorithms (ANFIS-GATLBO). The results of this study are described in the following.

5.1. Thermo-economic analysis

Station 1: New Delhi, India

For this station, data reveals that the minimum levelized COE (13.65 $/kWh) is obtained for scenario 6 (design point DNI of 550 W/m^2 and SM of 2.4). For this scenario, the optimum number of heliostats, tower height, receiver height and receiver diameter that were obtained were 14229, 233.98 m, 23.64 m, and 21.36 m, respectively. In addition, for scenario 6, the annual energy, capacity factor and net capital cost were obtained as 425.75 TWh, 54.0 % and 931.67 M$, respectively (see Table 6 below).

Figure 6 represents the different values of design point DNI and SM to assess the behaviour of annual energy (a) and levelized COE (b). Figure 6a shows that by decreasing the design point DNI and increasing the SM, the annual energy increases. Figure 6b indicates the lower values of levelized COE are seen for design point DNI from 500 to 750 and SM from 1.8 to 3.1 in which the minimum value is for design point DNI of 550 W/m^2 and SM of 2.4. After finding the optimum design point DNI and SM, the optimum value of solar field hours of storage is determined. Figure 6c illustrates that the minimum levelized COE and maximum capacity factor are obtained at TES hour of 12.

Table 6. Thermo-economic analysis of SPTS with different scenarios for station 1.

Scenario	Number of heliostats	Tower height (m)	Receiver height (m)	Receiver diameter (m)	Annual energy (kWh)	LCOE ($/kWh)	Capacity factor (%)	Net capital cost ($)
1	6434	175.107	17.726	15.026	168,152,912	23.03	21.3	593,042,496
2	7715	174.731	17.666	16.083	212,933,856	19.48	27.0	640,689,792
3	8815	182.057	18.026	17.060	249,834,064	17.65	31.7	640,689,792
4	10073	196.044	20.234	17.924	295,293,856	16.08	37.5	745,472,960
5	11706	216.696	21.484	20.180	357,804,576	14.52	45.4	823,022,592
6	***14229***	***233.989***	***23.640***	***21.367***	***425,755,456***	***13.65***	***54.0***	***931,677,568***
7	5414	155.730	15.175	14.015	134,979,504	26.52	17.1	541,413,760
8	6422	161.554	16.842	14.308	172,962,400	22.12	21.9	583,948,288
9	7092	179.959	17.745	16.204	203,052,128	19.91	25.8	622,032,640
10	8309	181.183	17.804	16.832	242,140,496	17.77	30.7	666,932,544
11	9707	197.305	19.943	17.922	292,727,328	15.97	37.1	732,168,128
12	11852	208.935	20.748	19.805	360,297,280	14.38	45.7	820,673,728
13	4029	134.802	13.448	12.287	93,343,800	34.48	11.8	477,888,928
14	4821	136.544	13.460	13.460	120,020,360	28.25	15.2	507,768,320
15	5299	156.460	15.145	14.183	143,875,264	24.78	18.2	538,152,256
16	6094	165.270	16.580	14.840	17,366,9200	21.74	22.0	574,712,512
17	7202	170.268	16.969	15.831	212,163,264	18.99	26.9	618,789,888
18	8783	180.707	17.375	17.448	261,922,224	16.80	33.2	683,491,648
19	7786	172.672	16.397	17.380	201,561,680	20.63	25.6	643,071,104
20	9037	192.679	18.278	18.524	255,309,328	17.65	32.4	703,620,352
21	10335	199.004	19.293	18.320	295,499,872	16.22	37.5	753,260,928
22	11841	210.983	21.972	18.963	348,509,888	14.87	44.2	821,707,136
23	13566	242.876	24.008	21.959	410,177,600	13.96	52.0	917,062,592
24	16754	247.743	25.316	22.644	463,907,520	13.80	58.8	1,037,314,816
25	20186	269.669	27.963	24.421	495,566,432	14.61	62.9	1,189,403,392
26	23699	295.140	29.485	26.806	508,465,632	15.98	64.5	1,350,711,424
27	27400	314.908	31.349	28.533	514,237,856	17.57	65.2	1,516,650,880

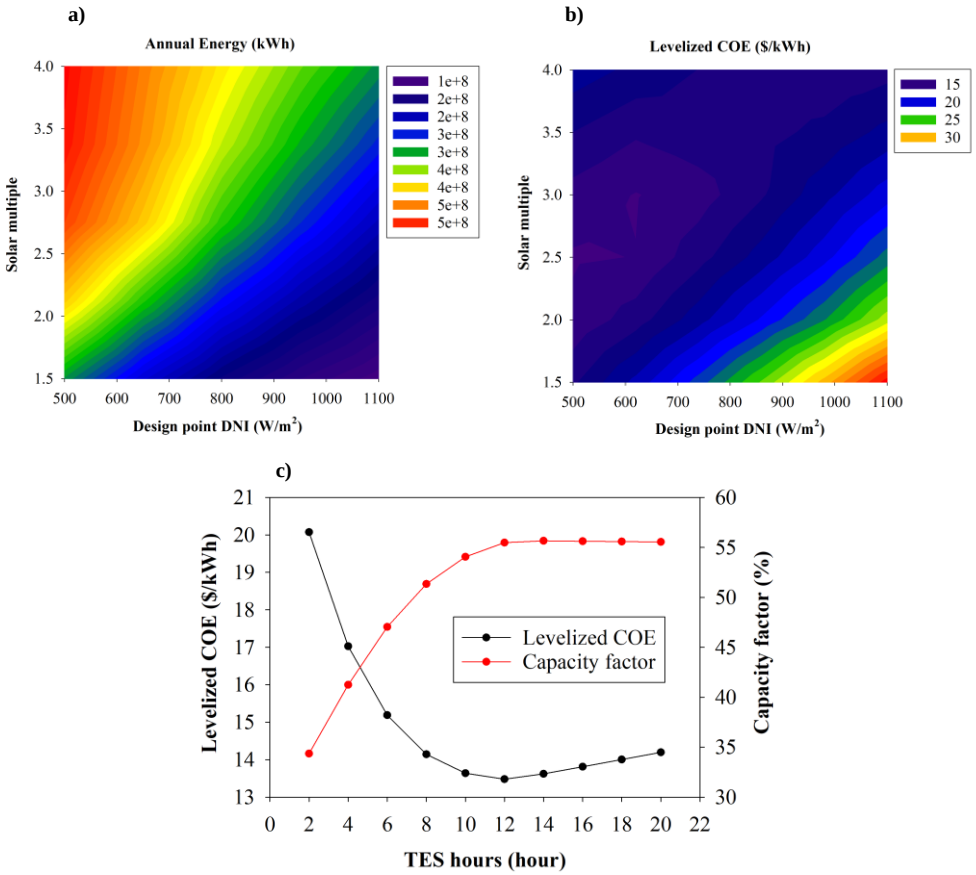

Fig. 6. Variation of annual energy (a), levelized COE (b) versus design point DNI and solar multiple; variation of levelized COE and capacity factor versus TES hours (c).

Station 2: Thanjavur, India

Data obtained from this station shows that the minimum levelized COE occurs in the scenario 5 with design point of 650 W/m^2 and SM of 2.4 (see Table 7 below). In this station the minimum levelized COE obtained is 10.88 $/kWh, which is lower than that for New Delhi. For this scenario, the number of heliostats, tower and receiver heights, and receiver diameter were obtained as 11644, 225.483 m, 21.4137 m and 19.6839 m, respectively. In addition, the capacity factor and net capital cost were achieved as 61% and 822 M$, respectively. In addition, the SPTS in this region can produce 480.94 TWh electricity.

Table 7. Investigation of STPS with different scenarios for station 2 (Thanjavur in India).

Scenario	Number of heliostats	Tower height (m)	Receiver height (m)	Receiver diameter (m)	Annual energy (kWh)	LCOE ($/kWh)	Capacity factor (%)	Net capital cost ($)
1	6436	178.008	16.962	14.592	254,683,584	15.23	32.3	588,898,816
2	7534	193.803	18.771	15.373	311,683,712	13.41	39.5	640,429,120
3	8561	204.058	19.219	16.740	362,869,312	12.27	46.0	686,636,224
4	9817	217.014	20.519	17.482	422,079,520	11.31	53.3	742,418,240
5	***11644***	***225.483***	***21.413***	***19.683***	***480,945,344***	***10.88***	***61.0***	***822,385,600***
6	13989	249.363	23.824	21.386	515,682,560	11.33	65.4	931,495,104
7	5304	169.814	15.674	13.480	207,385,248	17.33	26.3	539,585,600
8	6293	172.966	16.165	14.045	254,698,304	15.00	32.3	577,999,616
9	7136	180.262	17.838	14.708	296,735,872	13.64	37.6	617,079,104
10	8206	190.707	18.349	16.101	348,662,368	12.41	44.2	664,542,144
11	9619	207.802	19.181	18.196	416,069,248	11.32	52.8	730,598,848
12	11398	239.248	22.161	19.028	474,959,392	10.98	60.2	819,937,408
13	4121	130.433	13.378	10.991	146,648,688	21.97	18.6	475,119,136
14	4781	143.481	13.812	12.952	184,364,192	18.53	23.4	508,476,992
15	5275	164.440	15.653	12.934	215,219,936	16.60	27.3	535,269,952
16	6017	174.384	17.361	13.171	252,828,352	14.91	32.1	568,881,344
17	6993	192.633	18.412	15.393	303,427,296	13.41	38.5	620,487,936
18	8500	206.651	19.328	16.452	353,002,336	12.57	44.8	684,609,344
19	7682	182.727	18.110	15.527	303,301,568	13.79	38.5	641,215,616
20	8902	208.598	20.421	15.987	368,173,024	12.30	46.7	700,629,888
21	10038	219.924	21.447	17.091	423,702,336	11.41	53.7	752,781,376
22	11496	235.548	22.303	18.798	472,531,936	11.05	59.9	820,872,384
23	13651	243.671	23.697	20.878	507,338,144	11.32	64.4	914,012,416
24	16662	258.785	26.693	21.820	533,081,024	12.10	67.6	1,041,758,400
25	20423	269.232	26.776	25.191	544,235,648	13.41	69.0	1,196,476,544
26	23650	304.379	29.005	27.135	555,731,904	14.72	70.5	1,357,449,216
27	27880	310.173	31.840	28.215	558,240,960	16.34	70.8	1,529,398,400

It was also observed that the annual energy has a tendency to increase by increasing the SM and decreasing design point DNI (see Fig. 7a). Furthermore, the lower magnitudes of levelized COE are obtained for the SM in the range of 2 and 2.9 and design point DNI in the range of 600 and 800 W/m^{2}-(see Fig 7b). For this station, the minimum levelized COE is obtained with TES hour of 12 (Fig. 7c).

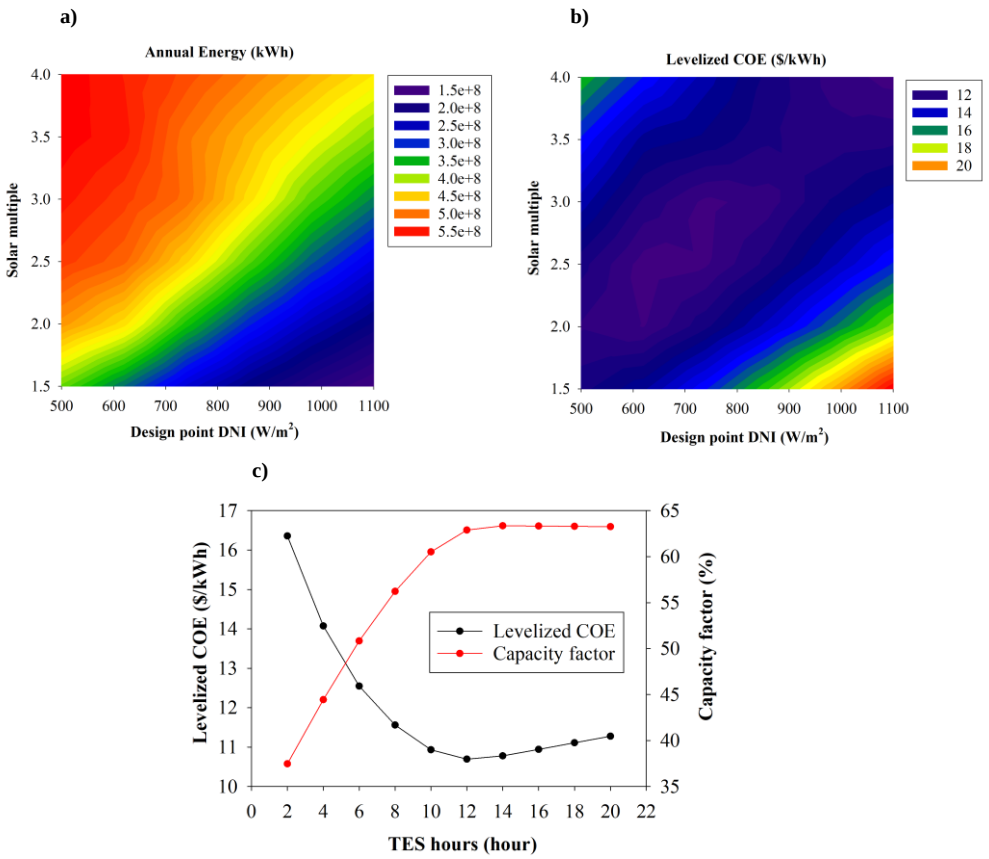

Fig. 7. The values of annual energy (a) and levelized COE (b) against design point DNI and SM; variation of levelized COE and capacity factor against TES hours (c).

Station 3: Dhaka, Bangladesh

Scenario 6 with design point of 550 W/m^2 and SM of 2.4 has shown the minimum levelized COE with 14.45 $/kWh see table 8 below). For this scenario, the capacity factor was obtained as 50.9%. The maximum capacity factor was reported for scenario 27 with design point DNI of 500 w/m^2 and SM of 4. But for this case the levelized COE was reported as 18.69 $/kWh and the net capital cost was obtained as 1,516 M$. A comparison between scenario 6 and 27 shows that finding the best design parameters for simulating the SPTS can significantly decrease the cost of the system. In addition, the difference in capacity factor between these scenarios is only 10.3%.

Figure 8a shows the variation of annual energy against design point DNI and SM. The graph reveals that the maximum annual energy is found with the design point DNI between 500 and 600 W/m^2 and SM between 2.4 and 3.4. Figure 8b indicates that for magnitudes of design point DNI from 500 to 700 W/m^2 and SM from 2.2 to 2.6, energy is produced at a lower cost. Figure 8c also shows that the optimum value of TES hour (for this station 12) for designing the SPTS with which the minimum levelized COE is obtained.

Table 8. Investigation of SPTS by various scenarios for station 3, Dhaka in Bangladesh.

Scenario	Number of heliostats	Tower height (m)	Receiver height (m)	Receiver diameter (m)	Annual energy (kWh)	LCOE ($/kWh)	Capacity factor (%)	Net capital cost ($)
1	6367	180.524	17.410	15.026	159,303,968	24.23	20.2	591,020,544
2	7629	180.735	18.355	15.933	201,624,432	20.58	25.6	641,446,016
3	8811	182.154	18.415	16.161	236,501,152	18.57	30.0	683,661,504
4	10067	194.757	19.811	18.784	281,134,144	16.91	35.7	747,153,664
5	11629	222.191	21.467	20.704	339,777,376	15.30	43.1	825,153,088
6	***13970***	***243.386***	***23.949***	***21.884***	***401,186,565***	***14.45***	***50.9***	***930,551,680***
7	5430	154.909	14.071	14.890	128,677,488	27.79	16.3	541,094,272
8	6220	175.417	16.662	15.440	163,744,368	23.34	20.8	583,779,968
9	7096	178.344	17.945	15.804	19,260,0624	20.94	24.4	620,761,216
10	8276	180.470	17.815	16.673	228,818,704	18.73	29.0	664,597,504
11	9722	192.915	19.753	18.407	279,199,904	16.74	35.4	732,536,704
12	11685	215.513	22.537	19.056	339,772,416	15.23	43.1	820,687,168
13	4067	131.564	13.515	11.659	87,971,648	36.50	11.2	476,737,056
14	4735	143.368	14.116	13.229	114,520,256	29.67	14.5	509,343,232
15	5348	152.168	14.927	13.361	136,695,568	25.94	17.3	535,101,280
16	6194	161.078	14.354	15.433	165,910,640	22.63	21.0	571,484,736
17	7141	175.068	16.688	16.802	202,645,440	19.91	25.7	620,575,552
18	8636	186.609	18.760	17.202	247,991,232	17.74	31.5	684,336,896
19	7646	180.920	18.158	15.966	191,074,720	21.70	24.2	641,558,400
20	9034	189.631	20.590	16.347	239,122,880	18.78	30.3	701,702,016
21	10209	203.306	20.116	18.812	281,242,432	17.07	35.7	755,652,928
22	11762	215.757	20.871	20.172	331,682,816	15.62	42.1	822,039,872
23	13760	233.252	23.129	21.348	387,222,848	14.70	49.1	912,647,296
24	16703	247.778	25.502	22.429	435,196,832	14.66	55.2	1,035,217,920
25	20179	267.810	27.434	24.642	642,930,080	15.59	58.7	1,187,051,392
26	23615	294.682	29.754	27.988	475,299,552	17.12	60.3	1,354,511,232
27	27471	312.226	30.023	29.662	482,816,288	18.69	61.2	1,516,491,648

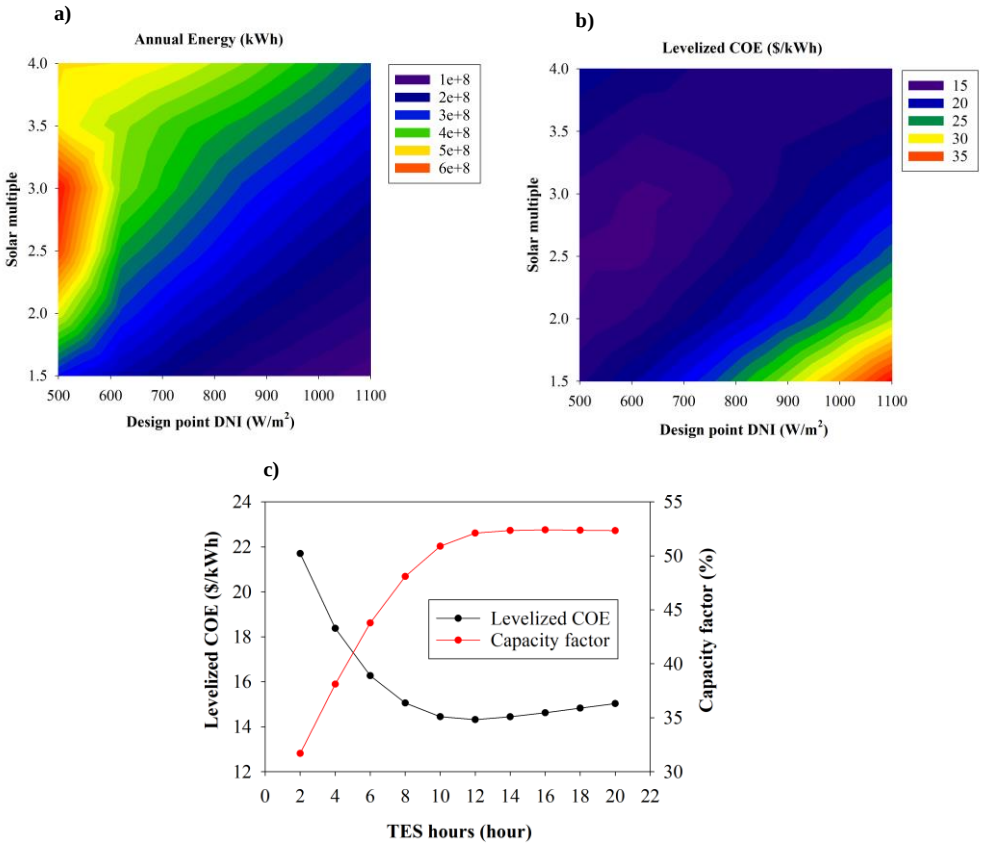

Fig. 8. The effect of design point DNI and SM over annual energy (a), levelized COE (b); the effect of TES hours over levelized COE and capacity factor (c).

Station 4: Kabul, Afghanistan

The minimum value of levelized COE (9.24 $/kWh) is obtained for scenario 4 (design point of 750 W/m^2 and SM of 2.4) as can be observed in Table 9. For this scenario, the capacity factor is reported to be 66.3%, which is higher than that for stations 1, 2 and 3. In addition, after the optimization process, the number of heliostats, tower and receiver heights, and receiver diameter were determined as 10084, 197.407 m, 19.49 m, and 18.47 m, respectively. Moreover, this SPTS can produce 522.59 TWh of electricity, which is higher than the other first three stations.

Table 9. Investigation of the SPTS for station 4 (Kabul, Afghanistan) by different scenarios.

Scenario	Number of heliostats	Tower height (m)	Receiver height (m)	Receiver diameter (m)	Annual energy (kWh)	LCOE ($/kWh)	Capacity factor (%)	Net capital cost ($)
1	6380	179.000	16.868	15.918	347,093,664	11.34	44.0	593,347,520
2	7773	173.276	16.544	17.240	419,354,240	10.09	53.2	643,302,656
3	8742	184.310	18.190	18.064	477,160,448	9.44	60.5	689,238,720
4	***10084***	***197.407***	***19.498***	***18.476***	***522,596,128***	***9.24***	***66.3***	***746,260,352***
5	11680	218.80	21.852	20.388	550,169,728	9.59	69.8	550,169,728
6	14255	233.937	23.114	21.567	555,046,016	10.55	70.4	931,627,776
7	5413	154.861	14.663	14.467	285,864,352	12.70	36.3	541,398,400
8	6374	164.182	16.788	14.820	344,173,408	11.30	43.7	585,024,960
9	7208	171.123	16.733	16.500	395,416,800	10.38	50.2	621,456,960
10	8308	180.170	17.832	16.960	459,620,576	9.53	58.3	667,301,312
11	9731	195.704	20.561	17.470	513,726,816	9.26	65.2	733,315,776
12	11713	215.976	21.444	20.189	542,898,560	9.68	68.9	823,147,328
13	4066	131.410	14.027	11.067	204,190,928	15.89	25.9	475,859,104
14	4835	136.711	13.388	13.024	249,187,632	13.80	31.6	508,278,848
15	5315	154.540	14.658	14.006	288,832,192	12.48	36.6	536,220,288
16	6223	157.081	15.398	14.080	337,979,872	11.27	42.9	570,725,120
17	7194	170.387	17.597	15.599	389,816,544	10.51	49.4	620,207,424
18	8821	180.752	17.586	16.528	425,820,672	10.45	54.0	682,206,784
19	7658	180.250	17.600	16.700	410,982,176	10.29	52.1	643,227,328
20	9002	192.110	19.312	17.744	483,785,504	9.47	61.4	703,170,624
21	10195	204.984	20.108	18.953	519,910,048	9.40	65.9	756,668,224
22	11726	217.696	22.089	19.672	545,168,832	9.66	69.1	824,963,712
23	13760	236.243	22.487	22.374	563,960,960	10.24	71.5	916,694,720
24	1658	247.731	24.283	22.715	566,746,176	11.36	71.9	1,037,283,904
25	20356	266.396	27.657	27.390	567,627,392	12.83	72.0	1,192,270,336
26	23721	297.500	29.094	27.349	572,702,656	14.27	72.6	1,355,211,648
27	27436	316.160	31.434	28.512	574,270,400	15.80	72.8	1,519,680,640

The annual energy production for the Kabul station increases by increasing design point DNI as well as SM (see Fig. 9). However, when calculating the levelized COE (Fig. 9b), it can be observed that this increase results in a rise in the cost of electricity generation. It is evident that for design point DNI between 600 and 1000 W/m^2 and SM between 1.8 and 3.2, the magnitudes of levelized COE are between 9 and 10 $/kWh. The optimum TES hour for this station was obtained at 14 (Fig. 9c).

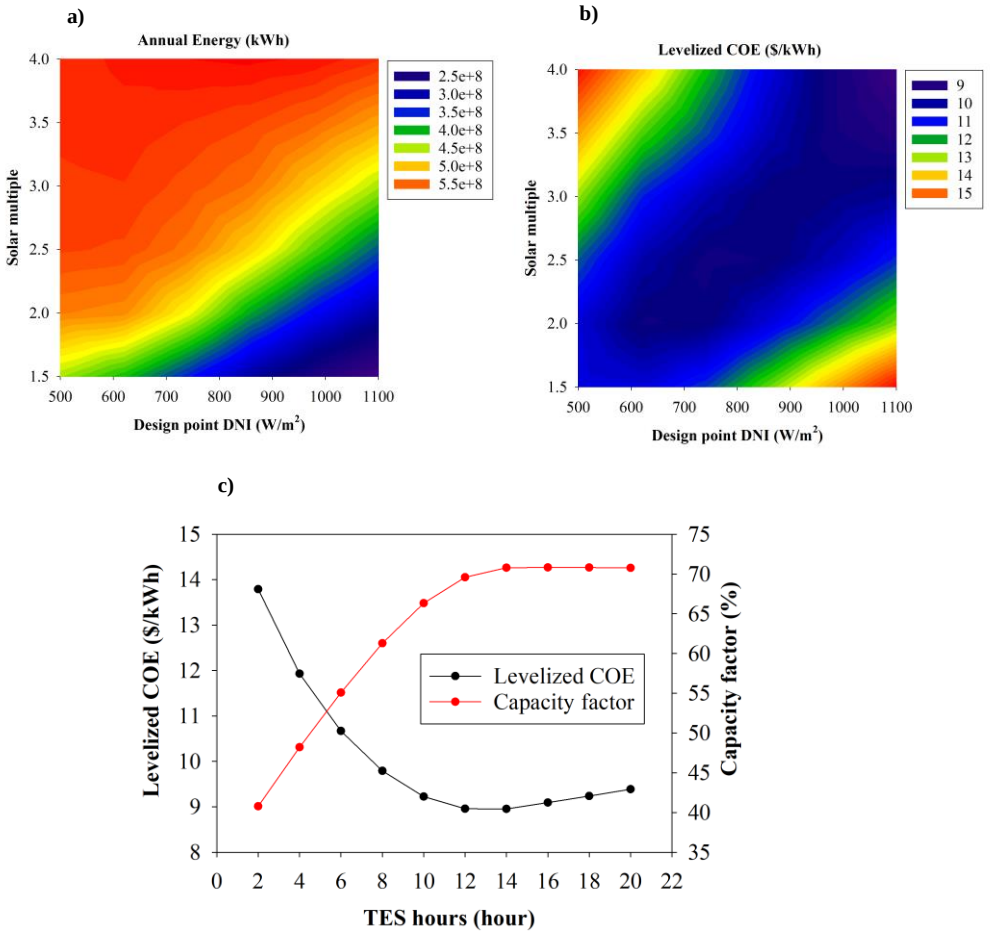

Fig. 9. The result of design point DNI and SM on annual energy (a), levelized COE (b); variation of levelized COE and capacity factor against TES hours in station 5, Islamabad Pakistan.

Station 5: Islamabad, Pakistan

Assessment was also conducted for station 5 with various scenarios (see Table 10). The results indicate that scenario 6 with design point of 550 W/m^2 and SM of 2.4 has shown the minimum levelized COE. Although Islamabad is in approximately the same geographical region as Kabul, the levelized COE for Islamabad was higher than that for Kabul. The capacity factor for this station in the minimum value of levelized COE was obtained as 61.9%, which is lower than Kabul and higher than Dhaka, Thanjavur and New Delhi.

For the Islamabad station, the annual energy production has the maximum value for design point DNI between 500 and 600 W/m2 and SM between 2.5 and 4 (Fig. 10a). When considering the economic impact, the lower values of levelized COE for design point DNI from 550 to 750 W/m2 and SM from 2.3 to 3 (see Fig. 10b). The optimum TES hour for this station is around 14 hours in which the minimum levelized COE as well as the maximum capacity factor are obtained (Fig. 10c).

Table 10. Assessment of the SPTS in Islamabad (Pakistan) by different scenarios.

Scenario	Number of heliostats	Tower height (m)	Receiver height (m)	Receiver diameter (m)	Annual energy (kWh)	LCOE ($/kWh)	Capacity factor (%)	Net capital cost ($)
1	6596	171.267	18.017	14.870	215,638,656	18.17	27.4	598,103,168
2	7792	179.896	17.546	16.486	266,741,376	15.74	33.8	646,285,120
3	8772	192.309	18.334	18.492	311,733,472	14.36	39.5	694,455,872
4	10051	209.153	20.440	19.361	368,270,656	13.12	46.7	756,198,016
5	11939	215.941	20.640	21.095	433,646,976	12.14	55.0	831,317,120
6	***14454***	***233.483***	***22.878***	***22.878***	***488,361,952***	***12.02***	***61.9***	***938,704,192***
7	5586	149.225	14.714	14.095	175,294,800	20.61	22.2	545,012,544
8	6453	168.112	15.825	15.994	219,000,640	17.68	27.8	589,491,392
9	7322	171.630	16.613	16.624	254,373,040	16.03	32.3	625,060,224
10	8424	180.567	18.094	16.611	298,710,560	14.53	37.9	670,516,096
11	9885	193.927	20.325	17.360	358,970,720	13.14	45.5	735,918,912
12	11870	221.408	20.197	22.031	435,066,272	12.13	55.2	833,679,232
13	4110	134.365	12.407	13.291	122,694,352	26.44	15.6	480,678,688
14	4821	142.495	13.798	13.367	154,221,664	22.19	19.6	511,388,288
15	5392	154.384	14.954	14.298	182,685,696	19.67	23.2	540,779,840
16	6264	159.405	15.461	14.867	217,566,464	17.44	27.6	575,469,632
17	7291	172.110	16.830	16.381	263,216,416	15.48	33.4	263,216,416
18	8831	186.634	18.665	16.978	317,756,032	14.02	40.3	690,159,872
19	7829	178.422	17.053	16.943	257,296,576	16.32	32.6	647,282,112
20	9276	186.615	17.770	18.708	315,548,320	14.43	40.0	708,650,816
21	10363	206.780	20.024	19.176	369,216,576	13.20	46.8	763,683,584
22	11927	215.384	22.176	19.597	425,922,272	12.34	54.0	830,312,064
23	14040	232.221	22.562	21.887	476,671,104	12.12	60.5	922,155,328
24	16964	251.982	25.974	22.716	513,352,672	12.64	65.1	1,050,520,704
25	20514	272.436	27.047	25.436	532,232,768	13.79	67.5	1,204,655,232
26	23986	301.776	29.028	27.744	539,458,560	15.29	68.4	1,370,381,824
27	27917	312.605	32.439	27.978	544,850,816	16.78	69.1	1,533,731,840

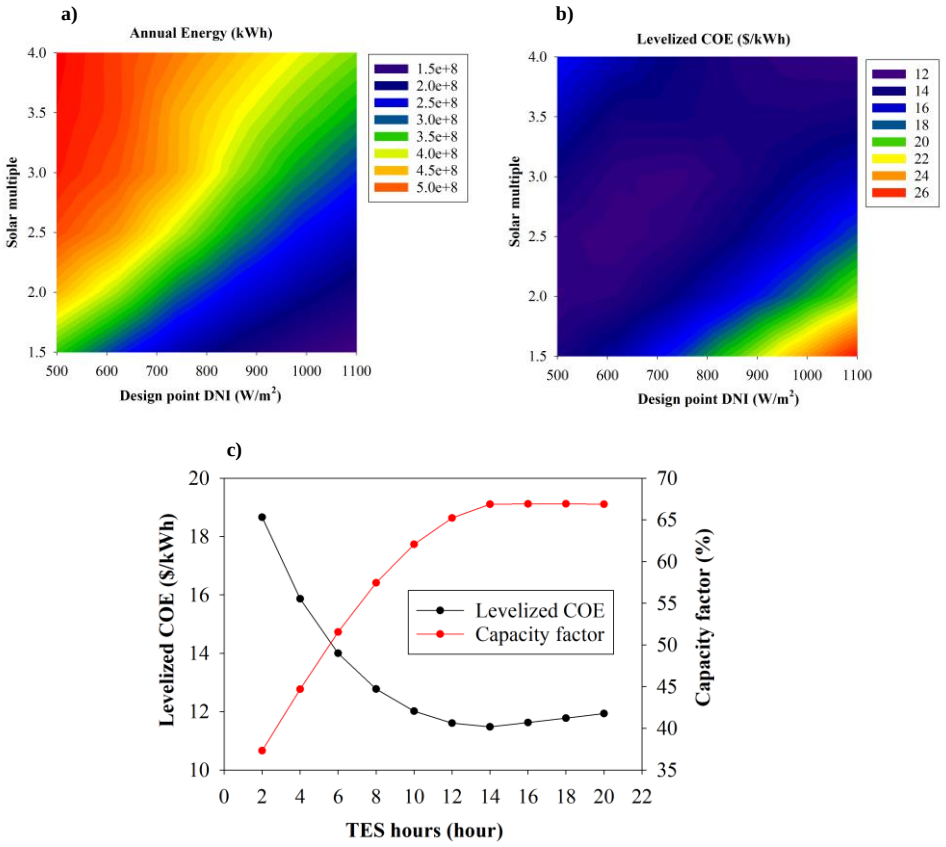

Fig. 10. The influence of design point DNI and SM on annual energy (a), levelized COE (b); variation of TES hours on levelized COE and capacity factor (c).

Optimization of Heliostat Field

For the ideal design of each station, the heliostat field is optimized. In addition, through the optimization process, the number of heliostats, tower and receiver heights, and receiver diameter and the position of each heliostat are determined. Figure 11 below represents the heliostat field for each station at optimum design.

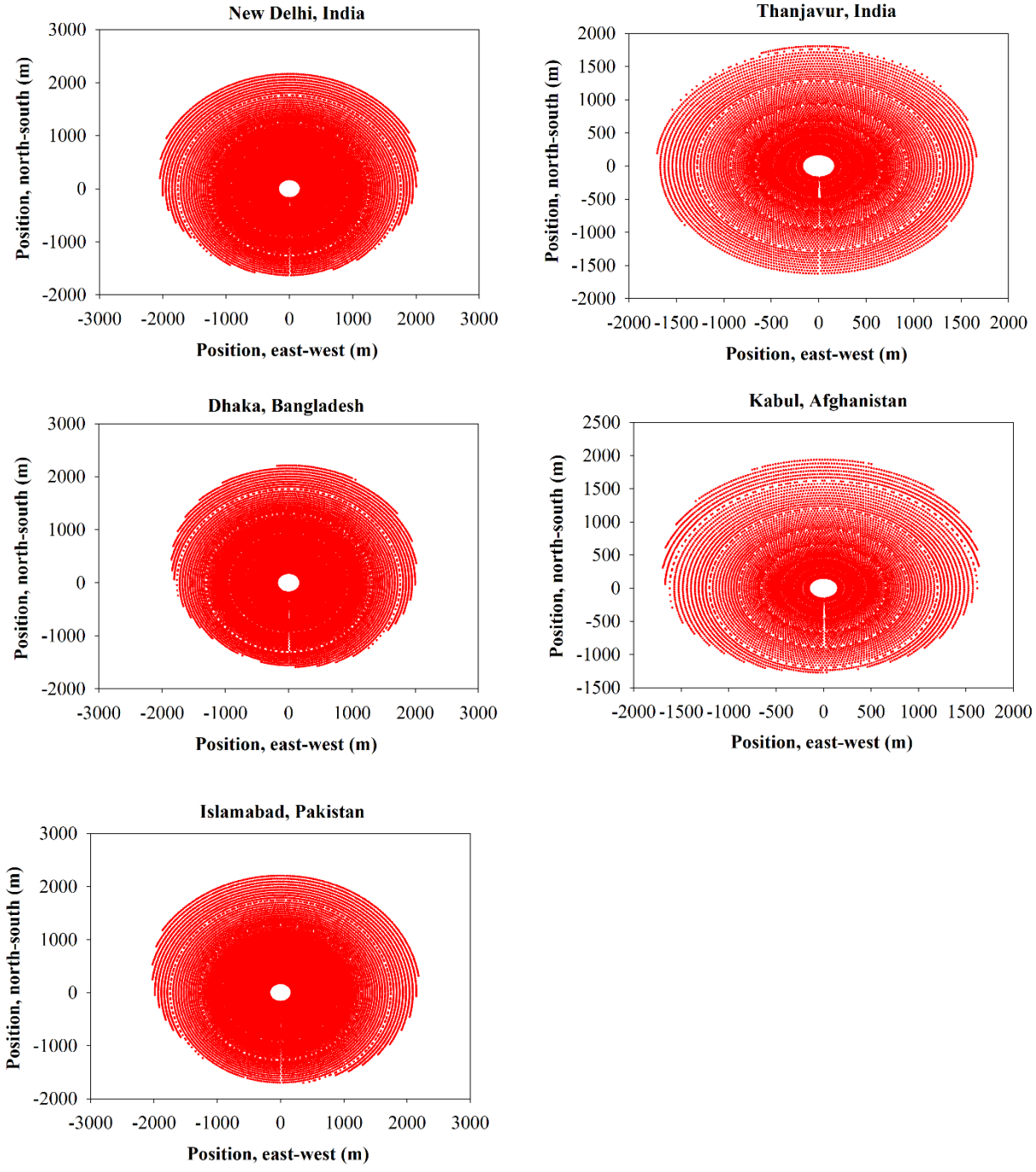

Fig. 11. A schematic of the heliostat field and position of the heliostats for the SPTDS system.

5.2. Artificial Intelligence Method

In this study, a SPTS for five stations situated in different locations around the world was simulated and assessed. The main contribution of the current study is developing an intelligent method (ANFIS optimized with a combination of GA and TLBO) for modelling the behaviour of a 100 MW SPTS for different stations and under different design parameters. The prediction of the performance of the proposed method was also compared with the performance of ANFIS-GA method. Furthermore, the model-based ANFIS was implemented by the following structures: the number of clusters for generating a fuzzy inference system was 10, maximum iteration was 500, number of population was 500, crossover percentage was 0.7, and the mutation rate was 0.2.

Prediction accuracy of the ANFIS-GATLBO and ANFIS-GA was reported in this paper (see Table 11). Both models were employed to predict the levelized COE, annual energy and capacity factor. It was found that for all cases the ANFIS-GATLBO performs better than ANFIS-GA for modelling the behaviour of the SPTS with different values of input parameters (see Table 11).

The statistical parameters employed for assessing the performance of the intelligent methods are root mean square error (RMSE), correlation coefficient (R) and determination coefficient (R^2) (see Appendix A for detailed description of these statistical criteria). To predict the levelized COE, the statistical indicators were obtained as RMSE=0.5363 $/kWh, R=0.9907 and R^2=0.9828 for the test data. In addition, the training and testing stages of the ANFIS-GATLBO and ANFIS-GA were reported (Fig. 12). It has been observed that data predicted by ANFIS-GATLBO follows the real data with low discrepancy in some instances.

In addition, a comparison of performance prediction of the ANFIS-GATLBO and ANFIS-GA employed for forecasting the annual energy produced by the SPTS was conducted (see Table 11). The correlation coefficients between data predicted by the intelligent model and real data indicate that the proposed hybrid ANFIS-GATLBO method is a powerful tool to simulate the behaviour of the SPTS for different stations and different values of design point DNI and SM (all R-values are beyond 0.99). Figure 13 illustrates the training and test phases of this prediction by both intelligent models, in which data predicted by ANFIS-GATLBO exactly conforms the real data. The proposed ANFIS-GATLBO was trained to predict the capacity factor through the input variables, and the appraisement of these predictions is summarized (see Table 11). The statistical indicators depict that the ANFIS-GATLBO successfully predict the capacity factor of the SPTS with RMSE=2.4340%, R=0.9902, and R2=0.9804. The training and testing phases for these predictions are shown in Fig. 14 below.

Table 11. Performance prediction of the ANFIS-GATLBO for modelling the SPTS.

	RMSE		R		R^2	
	Train	Test	Train	Test	Train	Test
ANFIS-GATLBO						
Levelized COE ($/kWh)	0.5046	0.5363	0.9955	0.9914	0.9910	0.9828
Annual Energy (kWh)	10736426.85	19029117.35	0.9971	0.9907	0.9942	0.9814
Capacity factor (%)	1.3354	2.5777	0.9970	0.9886	0.9940	0.9773
ANFIS-GA						
Levelized COE ($/kWh)	1.1206	1.4276	0.9744	0.9616	0.9494	0.9246
Annual Energy (kWh)	27252582.39	27954604.47	0.9807	0.9776	0.9617	0.9557
Capacity factor (%)	3.3998	3.5083	0.9813	0.9761	0.9629	0.9527

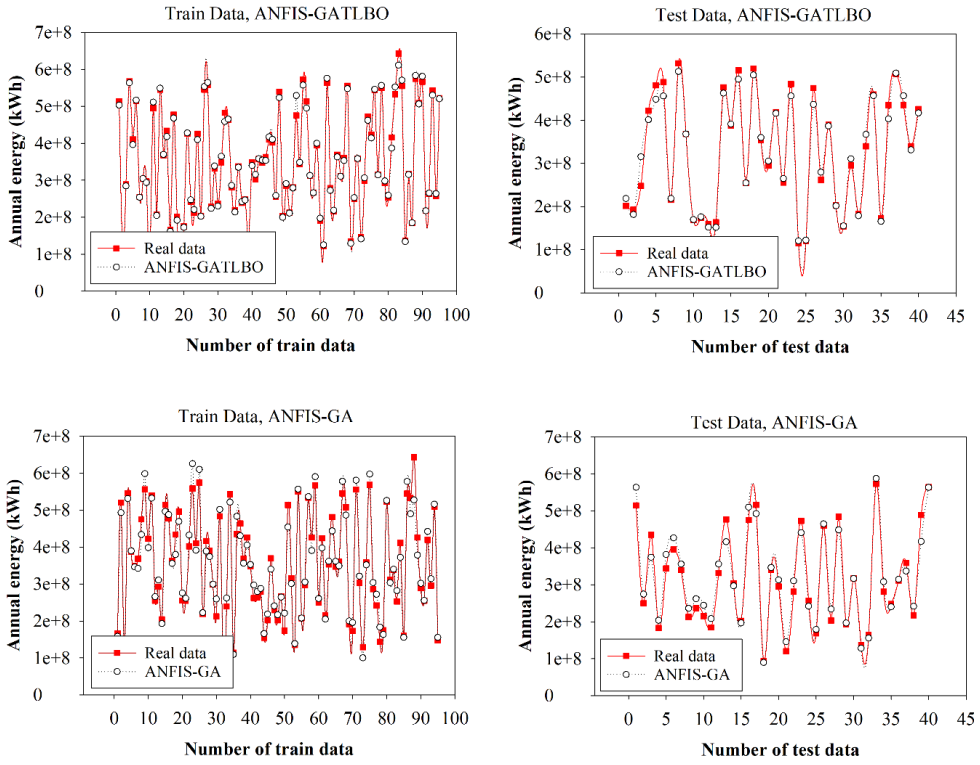

Fig. 12. Training and testing stages of the ANFIS-GATLBO and ANFIS-GA for forecasting the annual energy produced by the SPTS.

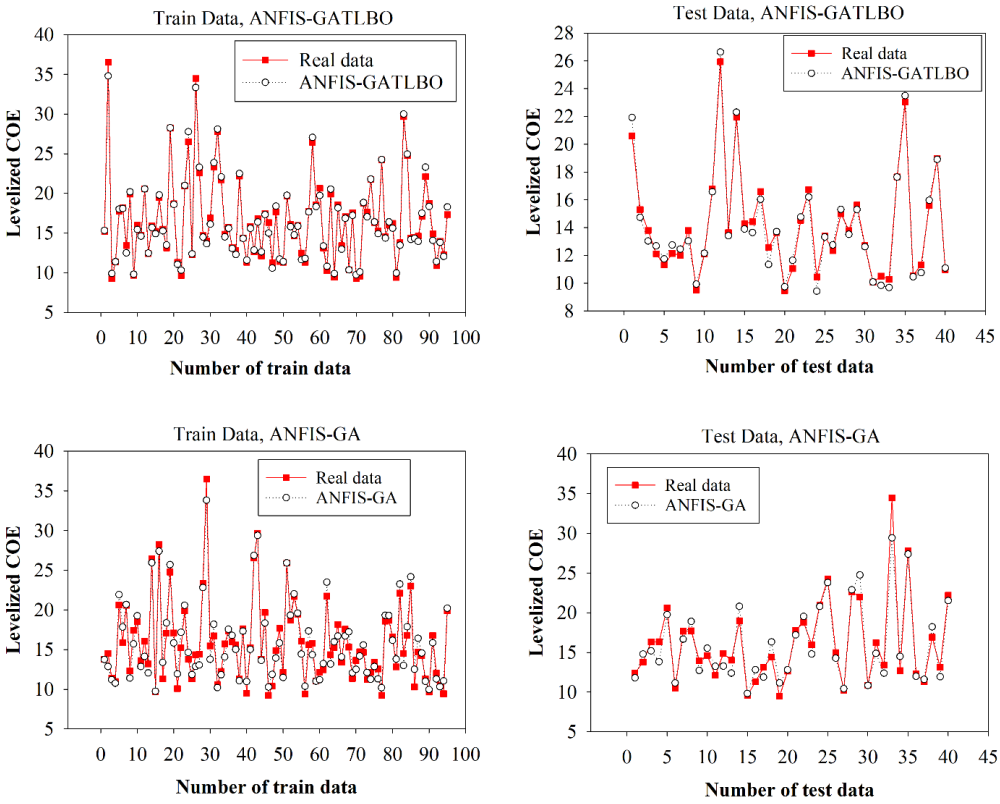

Fig. 13. Train and test data for ANFIS-GATLBO and ANFIS-GA for estimating the levelized COE.

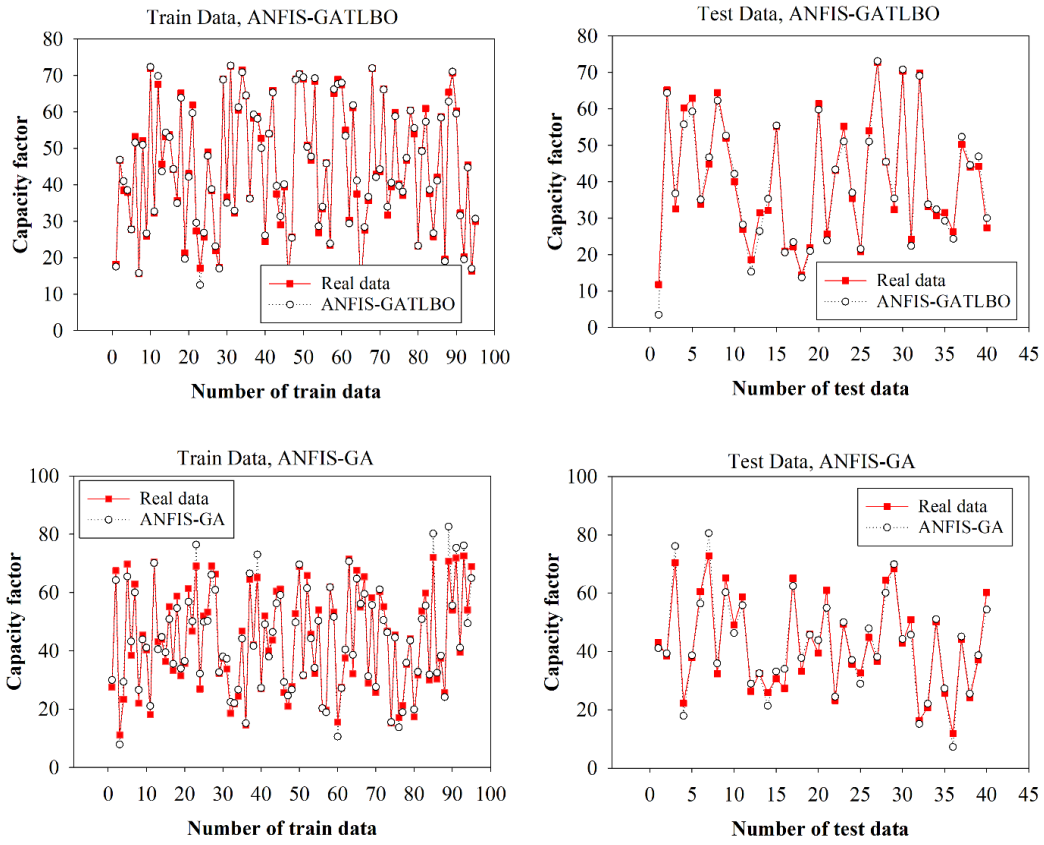

Fig. 14. Training and testing phases of the ANFIS-GATLBO and ANFIS-GA for predicting the capacity factor of the SPTS.

6. Conclusion

Although the energy efficiency of solar power tower system (SPTS) has been reported to be higher than other concentrating solar systems, such as linear Fresnel and parabolic trough, there are a number of parameters that need to be met to achieve the optimum operating conditions and system efficiency. Accordingly, in this study, we proposed an intelligent method for modelling a SPTS in which the main design parameters were considered as input parameters. The main conclusions of this study are that:

- The annual energy generated by the SPTS rose by increasing the SM and decreasing design point DNI. Nevertheless, the optimum design parameters should be determined while also considering the economic criteria. The minimum levelized COE was obtained in Kabul with 9.24 $/kWh. Likewise, the maximum capacity factor was obtained for this station (66.3 $/kWh).
- The optimum design parameters for each station are different. Therefore, the design point DNI and SM, along with the latitude and longitude of the stations, were considered as input variables to devise an intelligent network. This network created a non-linear relationship between the inputs and targets. The intelligent model was developed based on ANFIS, where a combination of GA and TLBO algorithms (ANFIS-GATLBO) markedly improved the performance prediction of the ANFIS. The results were compared with ANFIS-GA.

- The network was successfully trained with 70% of the dataset. This network was tested by 30% of the remaining data. The correlation coefficient (R) between the real data and predicted data for levelized COE, annual energy and capacity factor was obtained as 0.9914, 0.9907, and 0.9886 respectively.

To sum up, finding the optimal size of a SPTS (specifically for heliostat field and thermal energy storage) requires a comprehensive consideration of design parameters to reach the minimum levelized COE. This issue was fully addressed in this paper. Under a given power block size, for different stations, a network was proposed to create a relationship between the parameters. This network helps to obtain an appropriate design of the SPTS for different stations. In addition, the proposed network can be trained to determine the number of heliostats, tower height, receiver height, receiver diameter and net capital cost, based on the given data. These findings can contribute to enhancing system reliability and reducing the cost.

Appendix A

The performance of the intelligent methods is predicted with: root mean square error (RMSE, Eq. (A.1)), correlation coefficient (R, Eq. (A.2)) and determination coefficient (R^2, Eq. (A.3)).

$$RMSE = \sqrt{\frac{1}{n}\sum_{i=1}^{n}(x_i - y_i)^2} \tag{A.1}$$

$$R = \frac{\sum_{i=1}^{n}(x_i - \bar{x})(y_i - \bar{y})}{\sqrt{\sum_{i=1}^{n}(x_i - \bar{x})^2 \sum_{i=1}^{n}(y_i - \bar{y})^2}} \tag{A.2}$$

$$R^2 = \frac{n\sum_{i=1}^{n} x_i y_i - (\sum_{i=1}^{n} x_i)(\sum_{i=1}^{n} y_i)}{\sqrt{n(\sum_{i=1}^{n} x_i^2) - (\sum_{i=1}^{n} x_i)^2}\sqrt{n(\sum_{i=1}^{n} y_i^2) - (\sum_{i=1}^{n} y_i)^2}} \tag{A.3}$$

Acknowledgement

Ali Khosravi would like to express his appreciation to Aalto University (Department of Mechanical Engineering, Grant no. Post doc/T21201) for the financial support of this project.

References

[1] Khosravi A, Syri S, El Haj Assad M, Malekan M. Thermodynamic and Economic Analysis of a Hybrid Ocean Thermal Energy Conversion/Photovoltaic System with Hydrogen-Based Energy Storage System. Energy 2019;172:304–19.

[2] Khosravi A, Syri S, Zhao X, Assad MEH. An artificial intelligence approach for thermodynamic modeling of geothermal based-organic Rankine cycle equipped with solar system. Geothermics 2019;80:138–54. doi:10.1016/J.GEOTHERMICS.2019.03.003.

[3] Khosravi A, Nunes RO, Assad MEH, Machado L. Comparison of artificial intelligence methods in estimation of daily global solar radiation. J Clean Prod 2018;194:342–58.

doi:10.1016/J.JCLEPRO.2018.05.147.

[4] Khosravi A, Koury RNN, Machado L, Pabon JJG. Prediction of hourly solar radiation in Abu Musa Island using machine learning algorithms. J Clean Prod 2018;176:63–75.

[5] Amudam Y, Chandramohan VP. Influence of thermal energy storage system on flow and performance parameters of solar updraft tower power plant: A three dimensional numerical analysis. J Clean Prod 2019;207:136–52. doi:10.1016/J.JCLEPRO.2018.09.248.

[6] Ling-zhi R, Xin-gang Z, Yu-zhuo Z, Yan-bin L. The economic performance of concentrated solar power industry in China. J Clean Prod 2018;205:799–813. doi:10.1016/J.JCLEPRO.2018.09.110.

[7] Wei X, Lu Z, Wang Z, Yu W, Zhang H, Yao Z. A new method for the design of the heliostat field layout for solar tower power plant. Renew Energy 2010;35:1970–5. doi:10.1016/j.renene.2010.01.026.

[8] Benammar S, Khellaf A, Mohammedi K. Contribution to the modeling and simulation of solar power tower plants using energy analysis. Energy Convers Manag 2014;78:923–30. doi:10.1016/j.enconman.2013.08.066.

[9] Barigozzi G, Bonetti G, Franchini G, Perdichizzi A, Ravelli S. Thermal performance prediction of a solar hybrid gas turbine. Sol Energy 2012;86:2116–27. doi:10.1016/j.solener.2012.04.014.

[10] Aichmayer L, Spelling J, Laumert B, Fransson T. Micro Gas-Turbine Design for Small-Scale Hybrid Solar Power Plants. J Eng Gas Turbines Power 2013;135:113001. doi:10.1115/1.4025077.

[11] Spelling J, Laumert B, Fransson T. A Comparative Thermoeconomic Study of Hybrid Solar Gas-Turbine Power Plants. J Eng Gas Turbines Power 2013;136:011801. doi:10.1115/1.4024964.

[12] Xu E, Yu Q, Wang Z, Yang C. Modeling and simulation of 1 MW DAHAN solar thermal power tower plant. Renew Energy 2011;36:848–57. doi:10.1016/j.renene.2010.08.010.

[13] Pitz-Paal R, Botero NB, Steinfeld A. Heliostat field layout optimization for high-temperature solar thermochemical processing. Sol Energy 2011;85:334–43. doi:10.1016/j.solener.2010.11.018.

[14] Ozturk M, Dincer I. Thermodynamic assessment of an integrated solar power tower and coal gasification system for multi-generation purposes. Energy Convers Manag 2013;76:1061–72. doi:10.1016/j.enconman.2013.08.061.

[15] Avila-Marin AL, Fernandez-Reche J, Tellez FM. Evaluation of the potential of central receiver solar power plants: Configuration, optimization and trends. Appl Energy 2013;112:274–88. doi:10.1016/j.apenergy.2013.05.049.

[16] Singer C, Giuliano S, Buck R. Assessment of Improved Molten Salt Solar Tower Plants. Energy Procedia 2014;49:1553–62. doi:10.1016/j.egypro.2014.03.164.

[17] Besarati SM, Yogi Goswami D. A computationally efficient method for the design of the heliostat field

for solar power tower plant. Renew Energy 2014;69:226–32. doi:10.1016/j.renene.2014.03.043.

[18] Al-Sulaiman FA, Atif M. Performance comparison of different supercritical carbon dioxide Brayton cycles integrated with a solar power tower. Energy 2015;82:61–71. doi:10.1016/j.energy.2014.12.070.

[19] Collado FJ, Guallar J. Two-stages optimised design of the collector field of solar power tower plants. Sol Energy 2016;135:884–96. doi:10.1016/j.solener.2016.06.065.

[20] AlZahrani AA, Dincer I. Design and analysis of a solar tower based integrated system using high temperature electrolyzer for hydrogen production. Int J Hydrogen Energy 2016;41:8042–56. doi:10.1016/j.ijhydene.2015.12.103.

[21] Atif M, Al-Sulaiman FA. Energy and exergy analyses of solar tower power plant driven supercritical carbon dioxide recompression cycles for six different locations. Renew Sustain Energy Rev 2017;68:153–67. doi:10.1016/j.rser.2016.09.122.

[22] Chen R, Rao Z, Liao S. Determination of key parameters for sizing the heliostat field and thermal energy storage in solar tower power plants. Energy Convers Manag 2018;177:385–94. doi:10.1016/j.enconman.2018.09.065.

[23] Zhang Q, Wang Z, Du X, Yu G, Wu H. Dynamic simulation of steam generation system in solar tower power plant. Renew Energy 2019;135:866–76. doi:10.1016/j.renene.2018.12.064.

[24] Kalathakis C, Aretakis N, Roumeliotis I, Alexiou A, Mathioudakis K. Simulation models for supporting the solar thermal power plant operator. Energy 2019;167:1065–73. doi:10.1016/J.ENERGY.2018.11.041.

[25] Lippke F. Direct Steam Generation in Parabolic Trough Solar Power Plants: Numerical Investigation of the Transients and the Control of a Once-Through System. J Sol Energy Eng 1996;118:9. doi:10.1115/1.2847958.

[26] Eck M, Steinmann W-D. Modelling and Design of Direct Solar Steam Generating Collector Fields. J Sol Energy Eng 2005;127:371. doi:10.1115/1.1849225.

[27] Montes MJ, Rovira A, Muñoz M, Martínez-Val JM. Performance analysis of an Integrated Solar Combined Cycle using Direct Steam Generation in parabolic trough collectors. Appl Energy 2011;88:3228–38. doi:10.1016/j.apenergy.2011.03.038.

[28] Birnbaum J, Feldhoff JF, Fichtner M, Hirsch T, Jöcker M, Pitz-Paal R, et al. Steam temperature stability in a direct steam generation solar power plant. Sol Energy 2011;85:660–8. doi:10.1016/j.solener.2010.10.005.

[29] González-Roubaud E, Pérez-Osorio D, Prieto C. Review of commercial thermal energy storage in concentrated solar power plants: Steam vs. molten salts. Renew Sustain Energy Rev 2017;80:133–48. doi:10.1016/j.rser.2017.05.084.

[30] Aurousseau A, Vuillerme V, Bezian J-J. Control systems for direct steam generation in linear

concentrating solar power plants – A review. Renew Sustain Energy Rev 2016;56:611–30. doi:10.1016/j.rser.2015.11.083.

[31] de Sá AB, Pigozzo Filho VC, Tadrist L, Passos JC. Direct steam generation in linear solar concentration: Experimental and modeling investigation – A review. Renew Sustain Energy Rev 2018;90:910–36. doi:10.1016/j.rser.2018.03.075.

[32] Prieto C, Rodríguez A, Patiño D, Cabeza LF. Thermal energy storage evaluation in direct steam generation solar plants. Sol Energy 2018;159:501–9. doi:10.1016/j.solener.2017.11.006.

[33] González-Gómez PA, Gómez-Hernández J, Briongos JV, Santana D. Thermo-economic optimization of molten salt steam generators. Energy Convers Manag 2017;146:228–43. doi:10.1016/j.enconman.2017.05.027.

[34] Gómez-Hernández J, González-Gómez PA, Briongos JV, Santana D. Influence of the steam generator on the exergetic and exergoeconomic analysis of solar tower plants. Energy 2018;145:313–28. doi:10.1016/j.energy.2017.12.129.

[35] Gómez-Hernández J, González-Gómez PA, Briongos JV, Santana D. Maximizing the power block efficiency of solar tower plants: Dual-pressure level steam generator. Appl Therm Eng 2018;144:583–92. doi:10.1016/j.applthermaleng.2018.08.054.

[36] Li J, Gao G, Kutlu C, Liu K, Pei G, Su Y, et al. A novel approach to thermal storage of direct steam generation solar power systems through two-step heat discharge. Appl Energy 2019;236:81–100. doi:10.1016/j.apenergy.2018.11.084.

[37] Lin M, Reinhold J, Monnerie N, Haussener S. Modeling and design guidelines for direct steam generation solar receivers. Appl Energy 2018;216:761–76. doi:10.1016/j.apenergy.2018.02.044.

[38] Yağlı H, Karakuş C, Koç Y, Çevik M, Uğurlu R, Koç A. Designing and exergetic analysis of a solar power tower system for Iskenderun region. Int J Exergy 2019;28:96. doi:10.1504/IJEX.2019.097273.

[39] Xu C, Wang Z, Li X, Sun F. Energy and exergy analysis of solar power tower plants. Appl Therm Eng 2011;31:3904–13. doi:10.1016/j.applthermaleng.2011.07.038.

[40] Garcia JJ, Garcia F, Bermúdez J, Machado L. Prediction of pressure drop during evaporation of R407C in horizontal tubes using artificial neural networks. Int J Refrig 2018;85:292–302. doi:10.1016/J.IJREFRIG.2017.10.007.

[41] Bosch JL, López G, Batlles FJ. Daily solar irradiation estimation over a mountainous area using artificial neural networks. Renew Energy 2008;33:1622–8. doi:10.1016/j.renene.2007.09.012.

[42] López G, Gueymard CA. Clear-sky solar luminous efficacy determination using artificial neural networks. Sol Energy 2007;81:929–39. doi:10.1016/j.solener.2006.11.001.

[43] Srikrishnan V, Young GS, Witmer LT, Brownson JRS. Using multi-pyranometer arrays and neural

networks to estimate direct normal irradiance. Sol Energy 2015;119:531–42. doi:10.1016/j.solener.2015.06.004.

[44] Khosravi A, Koury RNN, Machado L. Thermo-economic analysis and sizing of the components of an ejector expansion refrigeration system. Int J Refrig 2018;86:463–79. doi:10.1016/J.IJREFRIG.2017.11.007.

[45] Khosravi A, Machado L, Oliviera RN. Time-series prediction of wind speed using machine learning algorithms: A case study Osorio wind farm, Brazil. Appl Energy 2018;224:550–66.

[46] Khosravi A, Koury RNN, Machado L, Pabon JJG. Energy, exergy and economic analysis of a hybrid renewable energy with hydrogen storage system. Energy 2018;148:1087–102.

[47] Alnaqi AA, Moayedi H, Shahsavar A, Nguyen TK. Prediction of energetic performance of a building integrated photovoltaic/thermal system thorough artificial neural network and hybrid particle swarm optimization models. Energy Convers Manag 2019;183:137–48. doi:10.1016/J.ENCONMAN.2019.01.005.

[48] Mittal M, Bora B, Saxena S, Gaur AM. Performance prediction of PV module using electrical equivalent model and artificial neural network. Sol Energy 2018;176:104–17. doi:10.1016/J.SOLENER.2018.10.018.

[49] Yousif JH, Kazem HA, Alattar NN, Elhassan II. A comparison study based on artificial neural network for assessing PV/T solar energy production. Case Stud Therm Eng 2019;13:100407. doi:10.1016/J.CSITE.2019.100407.

[50] López G, Gueymard CA, Bosch JL, Rapp-Arrarás I, Alonso-Montesinos J, Pulido-Calvo I, et al. Modeling water vapor impacts on the solar irradiance reaching the receiver of a solar tower plant by means of artificial neural networks. Sol Energy 2018;169:34–9. doi:10.1016/j.solener.2018.04.023.

[51] System Advisor Model (SAM) | n.d. https://sam.nrel.gov/ (accessed March 13, 2019).

[52] Solar resource maps and GIS data for 180+ countries | Solargis n.d. https://solargis.com/maps-and-gis-data/download/brazil/ (accessed January 28, 2019).

[53] Wagner MJ. Simulation and Predictive Performance Modeling of Utility-Scale Central Receiver System Power Plants by. UNIVERSITY OF WISCONSIN – MADISON, 2008.

[54] Turchi CS, Heath G a. Molten Salt Power Tower Cost Model for the System Advisor Model (SAM) 2013:1–53.

[55] Buragohain M, Mahanta C. A novel approach for ANFIS modelling based on full factorial design 2008;8:609–25. doi:10.1016/j.asoc.2007.03.010.

[56] Rao R V., Savsani VJ, Vakharia DP. Teaching-learning-based optimization: A novel method for constrained mechanical design optimization problems. CAD Comput Aided Des 2011;43:303–15.

doi:10.1016/j.cad.2010.12.015.

[57] Rao R V., Savsani VJ, Vakharia DP. Teaching-Learning-Based Optimization: An optimization method for continuous non-linear large scale problems. Inf Sci (Ny) 2012;183:1–15. doi:10.1016/j.ins.2011.08.006.